Modeling of the Plastic Anisotropy of Textured Sheet

PH. LEQUEU and J. J. JONAS

An alternative is proposed to the classical crystallographic and continuum techniques for representation of polycrystal anisotropy. It involves the use of continuum yield criteria to reproduce the yielding behavior of a collection of disoriented grains displaying typical experimental spreads. It is shown that the anisotropic properties pertaining to single ideal orientations are readily assessed. Yield surfaces as well as strain rate $R(\theta)$ and yield stress $\sigma(\theta)/\sigma(0)$ ratios are calculated for polycrystalline materials displaying several texture components. The Taylor, Sachs, and Kochendörfer grain interaction models are used for this purpose, the last of which leads to the fastest computations because it permits the texture/plastic properties relationship to be described analytically. Such methods are particularly well suited to FEM and CAD-CAM calculations. The predictions obtained from the present analysis are compared to experimental observations reported in the literature.

I. INTRODUCTION

THE anisotropic properties of sheet metals have generally been described by two different methods, *i.e.*, either a crystallographic approach such as that based on the Bishop and Hill yield surface or a macroscopic analysis employing various continuum yield functions. According to the former, the deformation of a polycrystalline aggregate is assumed to be accommodated by the activation of slip systems, the type of which depends on the metal under consideration. The crystallographic nature of plastic deformation is thus directly accounted for. The necessary transition from a single crystal to a polycrystal is then carried out on the basis of knowledge of the orientation distribution of the crystals (*i.e.*, from the texture) as well as from the definition of a grain interaction model. By contrast, the analysis used in the continuum methods is completely different in spirit. In this case, no reference is made to the orientations of the individual grains, so that the approach remains essentially macroscopic. The yield locus of the polycrystal under consideration (from which the stress and strain rate characteristics are readily deduced) is described instead by an assumed analytical function, the parameters of which are determined experimentally. The anisotropic behavior of the aggregate is thus accounted for only through the characteristics of the yield surface and not by means of the crystallographic texture of the material which is recognized to be the primary source of plastic anisotropy.

The validity and limitations of these two approaches are discussed in detail in Reference 1, with particular attention being paid to their use in the control of metal forming processes. The crystallographic methods are generally unsuitable for the rapid assessment of macroscopic properties, whereas the continuum techniques, because of their simple formulations, frequently fail to reproduce adequately some significant features of the plastic anisotropy.

Recently, Montheillet *et al.*[2] have proposed an alternative method, known as the continuum mechanics of textured polycrystals or CMTP, which combines aspects of both the previous approaches. This treatment is based on a modification of Hill's anisotropic continuum theory which permits the observed ideal orientations to be linked directly with the consequent plastic anisotropy of the material. The macroscopic stress and strain rate characteristics can thus be readily obtained from knowledge of the texture components displayed by the polycrystal. In this paper, the various grain interaction models used in such modeling are first discussed, followed by a description of the basic principles of the method. Some CMTP yield surfaces, as well as the strain rate and yield stress ratios calculated from them, are then presented and compared with experimental observations taken from the literature.

II. LOADING CONDITIONS AND GRAIN INTERACTION MODELS

The principal problem associated with the definition of a grain interaction model consists of determining the kind of averaging technique which should be used over the complete grain orientation distribution to assess the mean value of a given property. In this section, the mean yield stress and strain rate ratio, as assessed by a tensile test carried out at an angle θ to the sheet rolling direction (Figure 1), will first be considered. The following assumptions and notations are employed:

(i) The polycrystal, designated by the superscript (p), is constituted of single crystals grouped in N ideal orientations, each of which is represented by the superscript (g).

(ii) The volume fraction of crystals having a given orientation g is denoted α_g, such that $\sum_{g=1}^{N} \alpha_g = 1$.

(iii) The tensile specimen and crystal $\langle 100 \rangle$ axes are referred to as the (S) and (C) reference frames, respectively.

(iv) The transformation matrix from the (C) to the (S) axes is named P and is a function of the angle θ as well as of the orientation $\{hkl\}\langle uvw \rangle$ of the crystal orientation of interest (where $\{hkl\}$ and $\langle uvw \rangle$ are crystallographic directions parallel to the normal and rolling directions, respectively).

(v) The yield surface of a single crystal is represented by the function $F(\sigma_{ij(C)}) = 0$, where $\sigma_{ij(C)}$ refer to the stress components expressed in the $\langle 100 \rangle$ crystal axes.

The tensile test carried out to measure the yield stress and strain rate ratio is assumed to be represented by the following uniaxial stress tensor:

PH. LEQUEU, formerly Graduate Student, McGill University, Montreal, PQ, is with Research Center, Cegedur Péchiney, B.P. 27, 38340 Voreppe, France. J. J. JONAS is CSIRA-NSERC Professor of Steel Processing, Department of Metallurgical Engineering, McGill University, Montreal, PQ, Canada, H3A 2A7.

Manuscript submitted October 30, 1986.

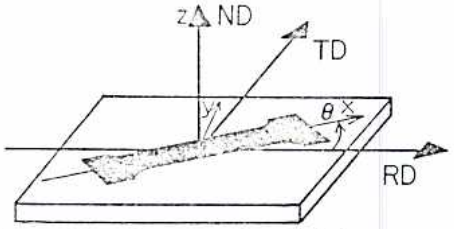

Fig. 1—System of coordinate axes for rolled sheet.

$$\boldsymbol{\sigma}_{(S)}^{(p)} = \begin{bmatrix} \sigma_{11(S)}^{(p)} & 0 & 0 \\ 0 & 0 & 0 \\ 0 & 0 & 0 \end{bmatrix} \quad [1]$$

The associated strain rate tensor is of the general form:

$$\dot{\boldsymbol{\varepsilon}}_{(S)}^{(p)} = (\dot{\varepsilon}_{ij(S)}^{(p)} \quad [2]$$

However, in the particular case of specimens cut from a sheet plane, the two additional conditions $\dot{\varepsilon}_{13(S)}^{(p)} = \dot{\varepsilon}_{23(S)}^{(p)} = 0$ can be prescribed as long as the Z-axis (or normal direction; see Figure 1) is an axis of mirror symmetry.[3,4] The $\dot{\varepsilon}_{11(S)}^{(p)}$ component is furthermore imposed as a test condition, say $\dot{\varepsilon}_{11(S)}^{(p)} = 1\ s^{-1}$. Recalling that the R-value is defined as

$$R = \dot{\varepsilon}_{22(S)}^{(p)} / \dot{\varepsilon}_{33(S)}^{(p)} \quad [3]$$

and that

$$\dot{\varepsilon}_{11(S)}^{(p)} + \dot{\varepsilon}_{22(S)}^{(p)} + \dot{\varepsilon}_{33(S)}^{(p)} = 0 \quad [4]$$

because of the assumed conservation of volume during plastic deformation, Eq. [2] can be rewritten as:

$$\dot{\boldsymbol{\varepsilon}}_{(S)}^{(p)} = \begin{bmatrix} 1 & \dot{\varepsilon}_{12(S)}^{(p)} & 0 \\ \dot{\varepsilon}_{12(S)}^{(p)} & -R/(1+R) & 0 \\ 0 & 0 & -1/(1+R) \end{bmatrix} \quad [5]$$

The quantities of interest here are $\sigma_{11(S)}^{(p)}$ and R, which have to be calculated under the assumptions listed above. As they pertain to a macroscopic reference frame (S) and as the crystallographic behavior is assumed to be known only through the function $F(\sigma_{ij(C)}) = 0$, a grain interaction model, such as one of the following, must be used.

A. *Uniform Strain (Taylor) Model*

In this case, each grain is assumed to undergo the same strain rate state as the polycrystal,[5] *i.e.*:

$$\dot{\varepsilon}_{ij(S)}^{(g)} = \dot{\varepsilon}_{ij(S)}^{(p)} \quad [6]$$

The stress state pertaining to the aggregate is then defined as:

$$\sigma_{ij(S)}^{(p)} = \sum_{g=1}^{N} \alpha_g \sigma_{ij(S)}^{(g)} \quad [7]$$

Here $\sigma_{ij(S)}^{(g)}$ is the point on the yield surface pertaining to the orientation g whose normal is $\dot{\varepsilon}_{ij(S)}^{(g)}$. The two unknowns in Eq. [5], R and $\dot{\varepsilon}_{12(S)}^{(p)}$, must be varied until the requirements of the loading conditions, *i.e.*, $\sigma_{ij(S)}^{(p)} = 0$ for $(i,j) \neq (1,1)$ are fulfilled. For this purpose, the strain rate tensor must be transformed into the (C) axes

$$\dot{\boldsymbol{\varepsilon}}_{(C)}^{(g)} = P \dot{\boldsymbol{\varepsilon}}_{(S)}^{(g)} \tilde{P} \quad [8]$$

where $\tilde{P}$ is the transpose of P. The flow rule expressed by:

$$\dot{\varepsilon}_{ij(C)}^{(g)} = \dot{\lambda}\, \partial F(\sigma_{ij(C)}) / \partial \sigma_{ij(C)} \quad [9]$$

must then be inverted in order to obtain the stress state $\sigma_{ij(C)}^{(g)}$. Finally, the averaging procedure specified by Eq. [7] is applied to the stress components transformed back into the specimen axes, $\sigma_{ij(S)}^{(g)}$.

As indicated above, when the uniform strain model is applied to the uniaxial tensile test, strain rate space must be swept by *two* parameters, and the computations that result are unreasonably long (see, for example, Reference 6). As an alternative, the testing conditions can be somewhat modified, an expedient which has been employed in crystallographic calculations as well.[3] For this purpose, the $\dot{\varepsilon}_{12(S)}^{(p)}$ component in Eq. [5] is assumed to be zero. As a consequence, the corresponding stress component $\sigma_{12(S)}^{(p)}$ can take on non-zero values, which are then incompatible with the boundary conditions at the free surface of the specimen. Such an approach, which utilizes a *non-uniaxial* testing representation, is valid only at the interior of the sample where the deformation is not generally homogeneous.

B. *Uniform Stress Direction (Sachs) Model*

Whereas the Taylor assumption is expressed entirely in terms of strain uniformity, the Sachs[7] model refers to the relation between the state of stress of an aggregate and its constituent grains. In this representation, the stress components pertaining to a given crystal are assumed to be proportional to the ones associated with the polycrystal: *i.e.*, the stress direction is assumed to be uniform across the various grains:

$$\sigma_{ij(S)}^{(g)} \propto \sigma_{ij(S)}^{(p)} \quad [10]$$

When Eq. [10] is employed in conjunction with the uniaxial tension loading conditions of Eq. [1], it is readily seen that only one unknown has to be determined in each grain, *i.e.*, $\sigma_{11(S)}^{(g)}$. This component is readily found by requiring the stress vector to lie on the yield surface as expressed in the specimen (S) axes. The overall yielding behavior is then derived from Eq. [7].

It is evident that the Sachs model permits only the mean stress state to be calculated. The mean strain rate, by contrast, remains unknown until some further assumptions are made. One possible way of calculating the R-value[8] consists of estimating the shape of the polycrystalline yield locus in the neighborhood of the uniaxial tensile direction, and then employing the normality rule to assess the corresponding strain rate. It should be noted, however, that the yield surface determined by this means (*i.e.*, at constant stress ratio) can be locally non-convex, so that the flow rule is not rigorously valid in these regions.

C. *Law of Mixtures (Kochendörfer) Model*

Another way of calculating the strain rate components pertaining to a textured polycrystal tested in uniaxial tension has been described by Kochendörfer.[9] Here the stress state is assumed to be the same as the one calculated from the Sachs model. The further hypotheses that are required for R-value calculations[9] are:

$$\dot{\varepsilon}_{11(S)}^{(g)} = \dot{\varepsilon}_{11(S)}^{(p)} \text{ imposed} \quad [11]$$

and

$$\dot{\varepsilon}^{(p)}_{ij(S)} = \sum_{g=1}^{N} \alpha_g \dot{\varepsilon}^{(g)}_{ij(S)} \qquad [12]$$

The normality rule expressed by Eq. [9] provides only the *direction* and not the *magnitude* of the strain rate vector. For this reason, it is necessary to impose an additional condition on the strain rate components for averaging purposes. This is done in the Kochendörfer analysis through the specification that the $\dot{\varepsilon}^{(g)}_{11(S)}$ must be the same for all the grains.

The Kochendörfer hypothesis provides a ready way of calculating the R-value pertaining to a textured aggregate. This is done by applying the normality rule (Eq. [9]) at the various loading points $\sigma^{(g)}_{(C)}$ (Sachs stress state) and using Eq. [11] for normalization purposes. The R-value is then evaluated from the averaging technique specified by Eq. [12] applied to the strain rate components which have been transformed back into the specimen axes.

III. BASIC PRINCIPLES OF THE CMTP METHOD

The classical crystallographic approach to yield surface prediction is based on the Bishop and Hill polyhedron, which pertains to single crystals displaying $\{111\}\langle 1\bar{1}0\rangle$ or $\{110\}\langle 111\rangle$ slip. If the operation of additional slip systems is assumed, other similar polyhedra are obtained, which also display faces, edges, and vertices.[10] As these yield functions are not readily differentiable, the normality principle (Eq. [9]) cannot be employed to give an analytical description of the stress/strain rate relationship. Furthermore, the yield surfaces defined from crystallographic considerations pertain only to perfect single crystals; thus the complete orientation distribution has to be considered for averaging purposes. Such an approach leads to extensive computations, and is unsuitable for on-line measurements or other rapid calculations.

The alternative model presented here considers that a polycrystal consists of collections of disoriented grains, each group being described by its own orientation and volume fraction. This is in turn related to the observation that a spread is generally found around the various texture components detected experimentally. The misorientation around a given ideal orientation is simulated[4] by means of a Gaussian distribution of scatter width ω_0, illustrated in Figures 2(a) through (c) for the $\omega_0 = 0$ deg (single crystal), $\omega_0 = 15$ deg, and random orientation distributions, respectively. The corresponding yield surfaces are calculated by the Bishop and Hill method, the π-plane and shear stress plane sections of which are given in Figures 2(d) through (i). It can be seen that, for typical experimental spreads of around 15 deg, the π-plane section is approximately circular, whereas the yield locus in shear stress space remains somewhat angular. Because of the circular nature of the π-plane section, the yielding behavior of such disoriented grains can be represented by analytical functions of the near quadratic type.[11]

The CMTP approach involves the following steps:

(i) The yield surface pertaining to a collection of *disoriented* grains is considered to be represented by an analytic function with parameters α_k

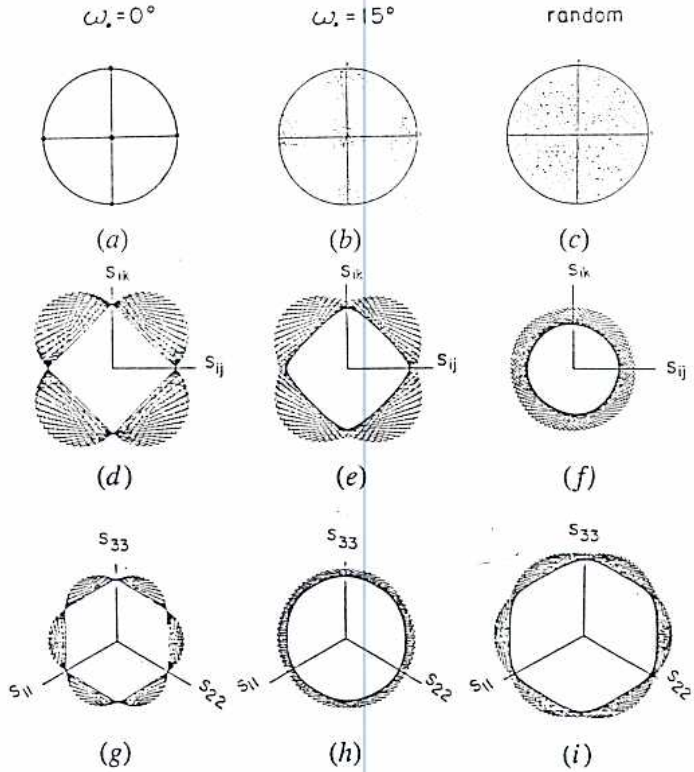

Fig. 2—(*a-c*) {100} pole figures; (*d-f*) cross-sections of the polycrystal yield locus containing two of the shear stress axes; and (*g-i*) π-plane sections of the polycrystal locus, corresponding to a 'perfect' single crystal with a scatter width $\omega_0 = 0$ deg, a 'disoriented' single crystal with a scatter width $\omega_0 = 15$ deg, and a random polycrystal, respectively.

$$F(S_{ij(C)}, \alpha_k) = 0 \qquad [13]$$

The latter is expressed in the $\langle 100\rangle$ axes of the ideal orientation of interest and $S_{ij(C)}$ are the components of the stress deviator tensor normalized by the critical resolved shear stress.

(ii) The parameters α_k of this yield criterion are estimated by means of a fitting procedure applied to the crystallographic loci. The details of this procedure are given in References 2, 8, 11, and 12.

A. *CMTP Yield Functions*

In the present work, two categories of yield function are used:

$$F_1(S) = \alpha_1\{|S_{11} - S_{22}|^n + |S_{11} - S_{33}|^n + |S_{22} - S_{33}|^n + 2\beta_1\{|S_{12}|^m + |S_{23}|^m + |S_{31}|^m\} = 1 \qquad [14]$$

$$F_2(S) = \alpha_2\{(S_{11} - S_{22})^2 + (S_{11} - S_{33})^2 + (S_{22} - S_{33})^2\} + 2\beta_2\{S_{12}^2 + S_{23}^2 + S_{31}^2\} + 2\gamma_2\{|S_{12}S_{13}| + |S_{12}S_{23}| + |S_{13}S_{23}|\} = 1 \qquad [15]$$

In the first case, the two different exponents n and m are introduced to take account of the different behaviors observed in the normal and shear stress sections (see Figure 2). The four parameters α_1, β_1, n, and m were calculated so that Eq. [14] gives a good fit to the Bishop and Hill yield surface pertaining to a collection of disoriented grains displaying a dispersion $\omega_0 = 15$ deg about the $\langle 100\rangle$ axes of the ideal orientation. Such a procedure leads to:

$$n = 2.6; \quad m = 1.5;$$
$$\alpha_1 = 0.49 \quad \text{and} \quad \beta_1 = 0.62 \qquad [16]$$

If the exponents n and m are prescribed to be equal so as to keep the yield function homogeneous in stress as well as to simplify the application of the Taylor hypothesis,[11] the following result is obtained:

$$n = m = 1.7;$$
$$\alpha_1 = 0.47 \quad \text{and} \quad \beta_1 = 0.54 \qquad [17]$$

The form of Eq. [15] is based on a development of the Bishop and Hill polyhedron, as discussed in more detail in Reference 8. The parameters $(\alpha_2, \beta_2, \gamma_2)$ were estimated in a manner similar to the one described above and a 'best' fit was obtained for:

$$\alpha_2 = 0.54; \quad \beta_2 = 0.60 \quad \text{and} \quad \gamma_2 = 0.20 \qquad [18]$$

B. *Comparison of the CMTP and Crystallographic Yield Surfaces for a Disoriented Crystal*

The validity of the present analytical representation will now be tested in two different ways:

(i) by comparing the CMTP and crystallographic yield surface sections pertaining to the crystal ⟨100⟩ axes; and
(ii) by comparing the corresponding stress and strain rate characteristics.

The shapes of the π-plane and shear stress plane yield surface sections are shown in Figures 3(a) and (b), respectively, for the three criteria described above. For comparison purposes, the crystallographic results corresponding to the $\omega_0 = 15$ deg orientation distribution are also given. It can be seen that there is fairly good agreement between the two types of loci. Nevertheless, the shear stress plane section corresponding to the $n = m = 1.7$ criterion is too rounded.

Plots such as those of Figure 3 give only limited information on the complete shape of the yield surface in the full five- or six-dimensional stress space. In particular, they do not throw any light on the yielding behavior in the mixed spaces where both normal and shear stresses are involved. For this purpose, more complex two- or three-dimensional sections have to be plotted. However, whereas such calculations are feasible in the case of the CMTP functions, they lead to lengthy computations when the Taylor/Bishop and Hill method is employed.

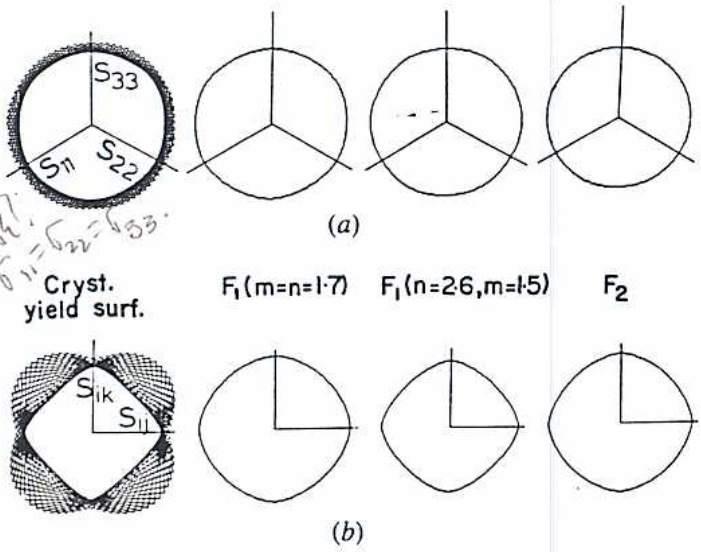

Fig. 3—(*a*) π-plane and (*b*) shear stress plane cross-sections of the crystallographic yield surface corresponding to a disoriented grain ($\omega_0 = 15$ deg) and of the F_1 ($n = m = 1.7$), F_1 ($n = 2.6, m = 1.5$) and F_2 yield functions.

C. *Comparison of the CMTP and Crystallographic Stress and Strain Rate Ratios for a Disoriented Crystal*

A complementary way of comparing the CMTP representation of a disoriented grain to the crystallographic model is to calculate the yield stress $\sigma_{11}(\theta)/\sigma_{11}(0)$ and strain rate $R(\theta)$ ratio curves for the two cases. The latter properties are obtained in tensile tests carried out along different directions θ in a {100} plane of the polycrystal under investigation.

For this purpose, the uniform strain assumption was applied to a set of 400 crystals representing a Gaussian distribution of scatter width $\omega_0 = 15$ deg about the reference orientation. The associated loading conditions were specified by the 'not-strictly-uniaxial' stress tensor ($\sigma_{12} \neq 0$) (see Section II–A). The results of the $R(\theta)$ computations are shown in Figure 4(a) for the F_1 ($n = m = 1.7$), F_2 (Eq. [15]), and crystallographic yield criteria. For comparison purposes, some experimental R-values reported by Viana and co-workers,[13] which pertain to a strong cube textured copper sheet, are also given. It can be seen that excellent agreement is observed with all three theoretical analyses.

The predicted stress ratio curves are illustrated in Figure 4(b). The CMTP and crystallographic approaches predict the same trends, *i.e.*, an increase followed by a decrease as the angle θ is increased from 0 to 90 deg, although the former representation calls for more variation than the latter. Some experimental values of $\sigma_{11}(\theta)/\sigma_{11}(0)$ taken from the work of Viana *et al.*[13,14] are also presented. The first set of values[13] (▲) is related to a very sharp cube texture (severity parameter* = 8.57); the specimen in this case is almost equivalent to a single crystal, as noted by the authors.[13] The second set of stresses[14] (▼) refers to a similar component, but with a texture severity of 5.64: *i.e.*, the cube orientation is more dispersed, as confirmed by the experimental pole figures. The stress ratio in the diagonal direction is observed to be much higher (0.98) than in the first example (about 0.77). Finally, the △ symbols characterize a cube textured sheet with a severity parameter of only 1.72. In this case, some secondary texture components are also present in the material. Figure 4(b) shows that a still higher stress ratio (1.05) pertains to a tensile test carried out at $\theta = 45$ deg on this material. The CMTP calculations are at best in qualitative agreement with the last data. This indicates that the CMTP criteria are more suitable for stress ratio predictions in materials with dispersed orientations (spreads of around 15 deg) than for 'near single crystal' components. It can also be seen that the crystallographic

*The severity parameter is defined as the standard deviation of the orientation distribution function with respect to that for a random material.

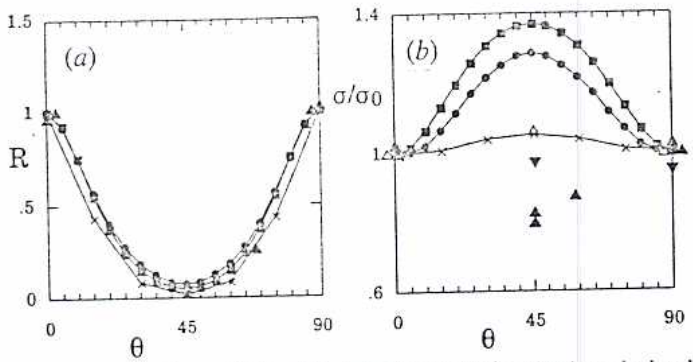

Fig. 4 — (*a*) Strain rate $R(\theta)$ and *b*) yield stress $\sigma(\theta)/\sigma(0)$ ratios calculated from the F_1 ($n = m = 1.7$) (—●●●—), F_2 (—■■■—), and crystallographic (—×××—) yield criteria for a collection of disoriented grains ($\omega_0 = 15$ deg). Experimental data (▲, ▼, △) from Refs. 13 and 14.

calculations corresponding to such dispersions are in good agreement with the last set of experimental values.

IV. YIELD SURFACES FOR TEXTURED SHEET

It was shown in the previous section that the strain rate ratios pertaining to a collection of disoriented grains can be obtained from simple analytical functions such as Eqs. [14] or [15] expressed in the ⟨100⟩ axes of the reference orientation. The trends in the yield stress ratios, on the other hand, appear to be overestimated. It will now be of interest to consider how this method can be applied when several ideal orientations (*i.e.*, several sets of disoriented grains) are present concurrently in a textured polycrystalline sheet. Under these conditions, the yield locus can be calculated as follows:

(i) For each set of grains (*i.e.*, for each ideal orientation), the analytical yield surface is reoriented into the testpiece axes by means of the texture information.

(ii) The loci reoriented in this way for the various texture components of the aggregate are averaged (on a volume fraction basis) using a suitable grain interaction model.

For this purpose, the yield surfaces are either combined: (i) at constant stress ratio (Figure 5(a)). Here the same stress direction applies to each crystal (Sach's technique); or (ii) at constant strain rate ratio (Figure 5(b)). In this case, all the grains are subjected to the same strain rate as the polycrystal (Taylor model).

In each case, the strain rate or stress ratio has to sweep the subspace of interest (shear stress plane, normal stress, or π-plane, *etc.* . . .) by increments, which can be varied depending on the desired accuracy of the solution. Three-dimensional loci can theoretically be treated in this way. However, the two-dimensional sweeping which is then necessary (a direction in three-dimensional space is characterized by two parameters) renders the computations unrealistically lengthy.[6] For this reason, only planar cross sections of the yield surfaces were calculated in this study.

A. *Contribution from the Randomly Oriented Grains*

A polycrystalline texture frequently cannot be realistically represented by a limited number of disoriented texture components. This is because as many as 10 to 20 pct of the grains remain randomly oriented in many deformed materials, as indicated by the more or less uniform 'background' observed in pole figures. For the present purpose, it is necessary to incorporate the effect of this random background by means of an analytic function representing the yield surface of a random polycrystal.

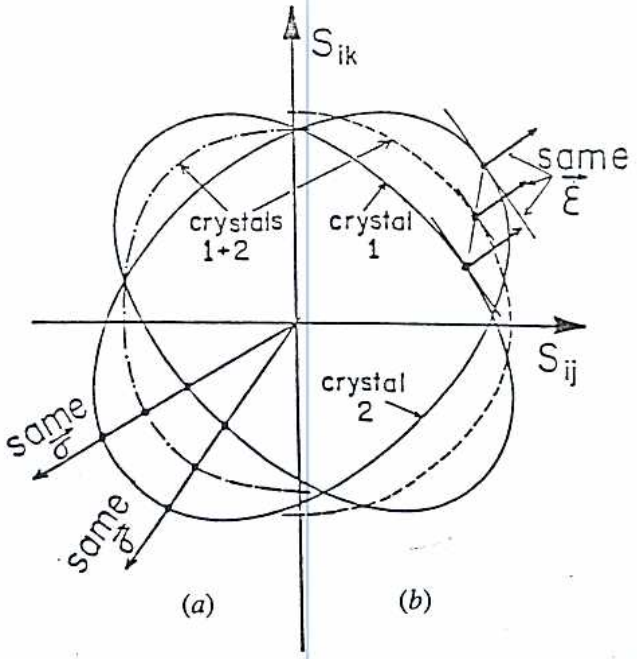

Fig. 5 — (*a*) Combination of two yield surfaces by the Sachs method. The crystals associated with each of the loci experience the same stress direction as the polycrystal. (*b*) Combination of two yield surfaces by the Taylor method. The crystals associated with each of the loci strain at the same rate as the polycrystal.

If the crystallographic loci of Figures 2(f) and 2(i) (random aggregate) are compared to the continuum surfaces, the following comments can be made:

(i) In the shear stress plane (S_{ij}, S_{ik}) $(i, j, k = 1, 2, 3)$, the yield locus of a randomly oriented polycrystal can be represented by a quadratic function

$$S_{ij}^2 + S_{ik}^2 = Y_1^2 \qquad i, j = 3, 4, 5 \qquad [19]$$

(ii) In the π-plane (S_{11}, S_{22}, S_{33}), the shape of the crystallographic surface suggests a representation of the form

$$|S_{22} - S_{11}|^n + |S_{11} - S_{33}|^n + |S_{33} - S_{22}|^n = Y_2^n \qquad [20]$$

It has been shown[8] that the above three parameters (Y_1, Y_2, and n) can be derived from knowledge of the Taylor factors in uniaxial ($M_T = 3.06$) and plane strain ($M_{PST} = 2.86$) tension and from some symmetry considerations. This leads to $Y_1 = 0.953\sqrt{6}\,\tau_c$, $Y_2 = 1.349\sqrt{6}\,\tau_c$, and $n \approx 9$. The analytical functions derived in this way can be used to represent the yielding behavior of a random aggregate in the *macroscopic* shear stress and normal stress planes, respectively. Similar exponents ($m = n = 6$ and $m = n = 8$) were derived by Hosford[15,16,17] to fit the yield surfaces pertaining to a random aggregate assuming {111}⟨110⟩ slip and ⟨111⟩-pencil glide, respectively.

B. *Comparison of the CMTP and Crystallographic Yield Surfaces Pertaining to Textured Polycrystals*

CMTP and crystallographic yield loci will now be calculated for actual textured materials. The two examples selected pertain to a Cu-20 pct Zn brass and an Al-killed steel sheet. For the CMTP calculations, the texture only needs to be decomposed into a small number of disoriented ideal orientations. The brass sheet, for example, can be considered[18] to consist of the Bs-$\{011\}\langle 2\bar{1}1\rangle$, Goss-$\{011\}\langle 100\rangle$, and random components in the volume fraction ratios 64.9:17.1:18.0. The steel studied by Parnière,[19] on the other hand, can be estimated to be made up of 46 pct $\{111\}\langle 1\bar{1}0\rangle$ + 23 pct $\{554\}\langle 225\rangle$ + 15 pct $\{310\}\langle 001\rangle$ + 8 pct $\{111\}\langle 11\bar{2}\rangle$ + 8 pct $\{100\}\langle 011\rangle$. By contrast, the crystallographic approach requires the complete orientation distributions of the grains, as noted above. In the present case, the latter were simulated by means of sets of 600 grains distributed according to the various texture components, volume fractions, and scatter widths observed experimentally (Figures 6(a) and (b)). The appearance of these representations is illustrated in Figures 6(c) and (d), from which it is evident that there is good agreement with the experimental pole figures.

The π-plane sections pertaining to these aggregates were calculated using both the Taylor and Sachs assumptions (Figure 5). The method described in the first part of this section was applied to the F_1 ($n = m = 1.7$) and F_2 continuum functions. The crystallographic loci, on the other hand, were evaluated by the classical tangent method described in References 3, 4, and 20. The results of these computations are presented in Figures 7 and 8 for the brass and Al-killed steel sheets, respectively.

As expected, the CMTP surfaces are considerably smoother than the crystallographic loci. Nevertheless, the F_2 predictions (Figures 7(c) and 8(c)) are somewhat less smooth than the F_1 loci (Figures 7(b) and 8(b)), and some rounded vertices as well as flatter regions can be detected. It is of interest that the general orientations of the CMTP surfaces are similar to those displayed in Figures 7(a) and 8(a). This is particularly striking for the case of the Cu-

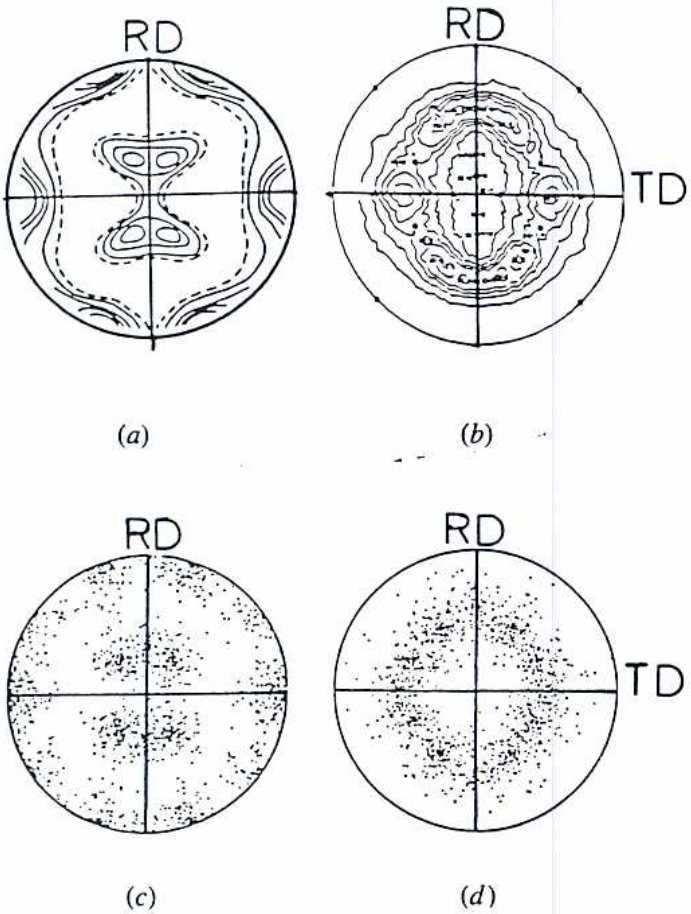

Fig. 6—(*a*) Experimental {111} pole figure for a Cu-20 pct Zn rolled sheet;[18] (*b*) experimental {100} pole figure for Al-killed steel.[19] (*c-d*) Corresponding pole figures simulated from the texture data (texture component + volume fraction + scatter width).

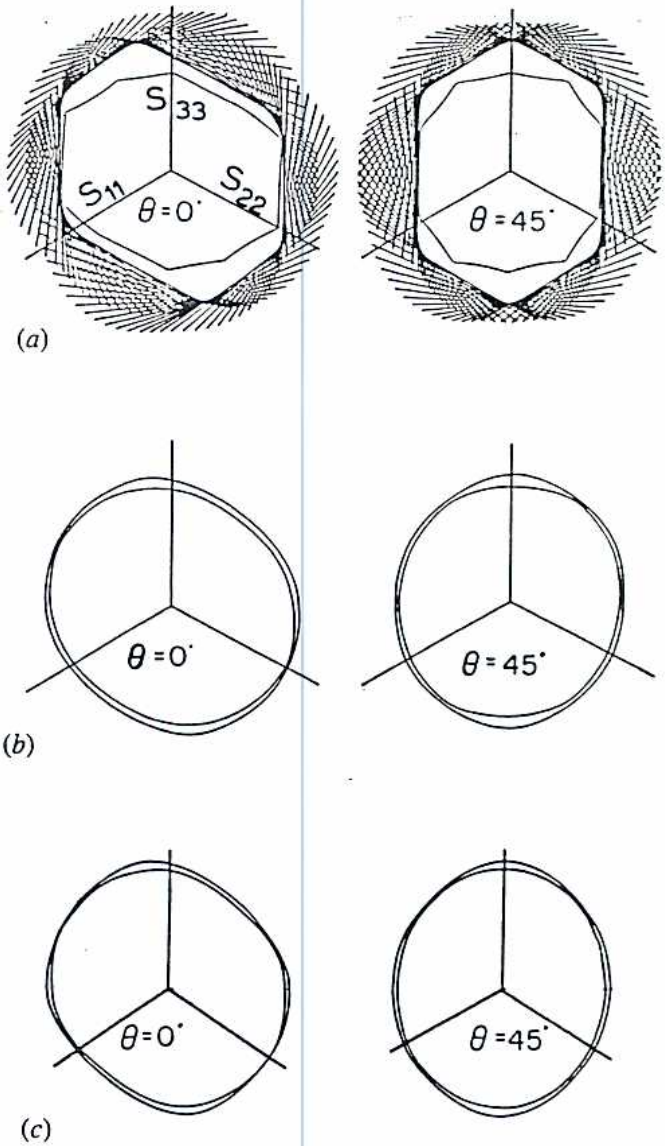

Fig. 7—π-plane yield surface cross-sections calculated for the Cu-20 pct Zn sheet of Fig. 6(a). θ refers to the angle between the S_{11} and rolling directions. (*a*) Crystallographic calculations based on the orientation distribution of Fig. 6(c); (*b*) and (*c*) CMTP predictions for the F_1 ($n = m = 1.7$) and F_2 yield criteria, respectively, corresponding to the following distribution:[18] 64.9 pct $\{011\}\langle 2\bar{1}1\rangle$ + 17.1 pct $\{011\}\langle 100\rangle$ + 18 pct random components.

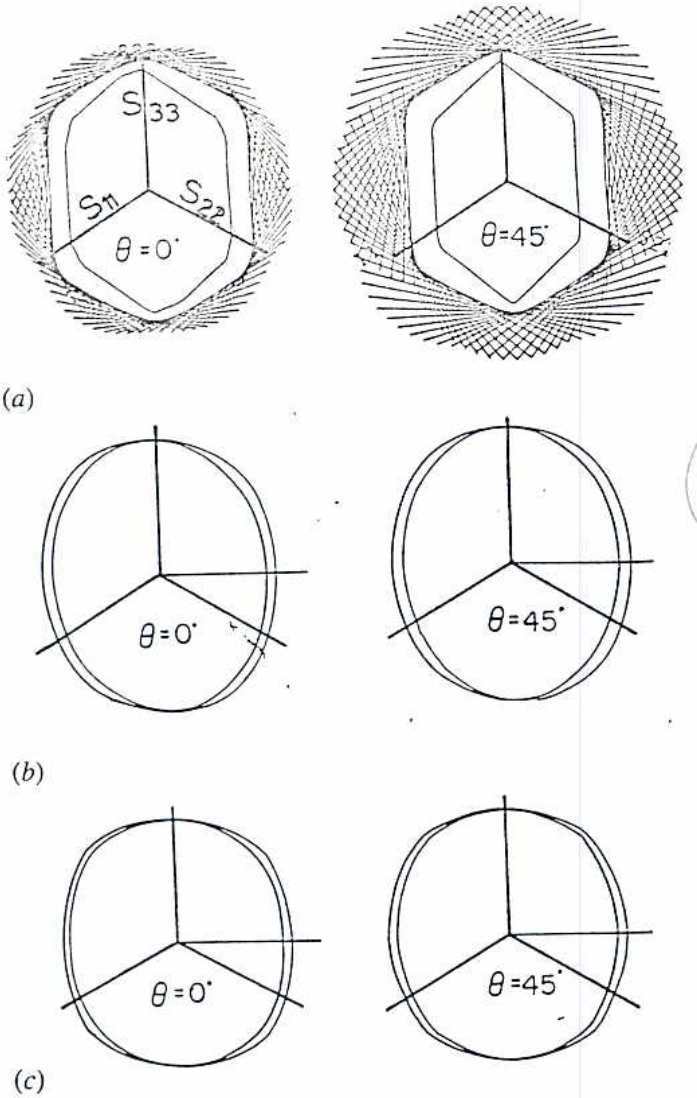

Fig. 8 — π-plane yield surface cross-sections calculated for the Al-killed steel sheet of Fig. 6(b). θ refers to the angle between the S_{11} and rolling directions. (*a*) Crystallographic calculations based on the orientation distribution of Fig. 6(d); (*b*) and (*c*) CMTP predictions for the F_1 ($n = m = 1.7$) and F_2 yield criteria, respectively, corresponding to the following distribution:[8] 46 pct $\{111\}\langle 1\bar{1}0\rangle$ + 23 pct $\{554\}\langle 22\bar{5}\rangle$ + 15 pct $\{310\}\langle 001\rangle$ + 8 pct $\{111\}\langle 11\bar{2}\rangle$ + 8 pct $\{100\}\langle 00\bar{1}\rangle$.

20 pct Zn at $\theta = 0$ deg, where the polycrystalline locus is oriented close to the $S_{11} = 0$ direction. Note also the lack of convexity of the Sachs combinations (inner loci of Figures 7(a) and 8(a)), which is incompatible with the thermodynamics of flow.

C. *Comparison of CMTP and Experimental Loci for Textured Polycrystals*

We turn now to a comparison between the CMTP predictions and experimentally determined yield surfaces. Here the experimental results of Viana *et al.*[13] (shown as tangent lines) are used together with their CODF data for a 70 pct cold rolled and annealed Ti-bearing steel. The texture components as well as their respective weights are taken from Reference 13. The results of these computations are shown in Figures 9(a) and (b) for the F_1 ($n = m = 1.7$) and F_2 criteria, from which the good agreement is evident.

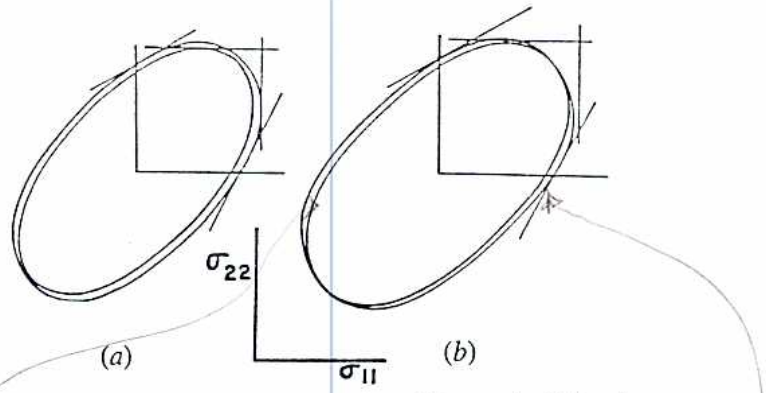

Fig. 9 — Comparison between the experimental (σ_{11},σ_{22}) yield surface cross-sections of Viana *et al.*[13] for a 70 pct cold rolled and annealed Ti-bearing steel and the predictions obtained from (*a*) the F_1 ($n = m = 1.7$) and (*b*) the F_2 criteria. The curves are normalized by the uniaxial yield stress σ_{11}. Texture data from Ref. 13. Outer locus: Taylor model; inner locus: Sachs model.

A similar set of results is presented in Figure 10 for the recrystallized aluminum tubes tested by Althoff and Wincierz.[21] Here the 1 and 2 axes refer to the tangential and axial directions, respectively. As suggested by the authors,[21] the texture was decomposed into four ideal orientations: $\{011\}\langle 1\bar{1}1\rangle$, $\langle 111\rangle$ fiber (approximated by equal parts of $\{112\}\langle 111\rangle + \{123\}\langle 111\rangle + \{134\}\langle 111\rangle$), $\{011\}\langle 611\rangle$ and $\{001\}\langle 310\rangle$ (where $\{hkl\}$ and $\langle uvw\rangle$ are parallel to the radial and axial directions, respectively) in the volume fraction ratios 5:3:1:1. The CMTP predictions normalized by the uniaxial tangential yield stress are again seen to be in good agreement with the measured loci. The experimental strain rate ratios (tangents to the locus) are also well approximated in this case. However, the near plane strain stresses ($\dot{\varepsilon}_{\text{tangential}} = 0$) are somewhat overestimated.

V. THE PLASTIC PROPERTIES OF TEXTURED SHEET

The stress and strain rate characteristics of a metal workpiece can be readily deduced from knowledge of its yield surface. More specifically, the locus size gives the amplitude of the stresses, whereas its shape leads to the values of

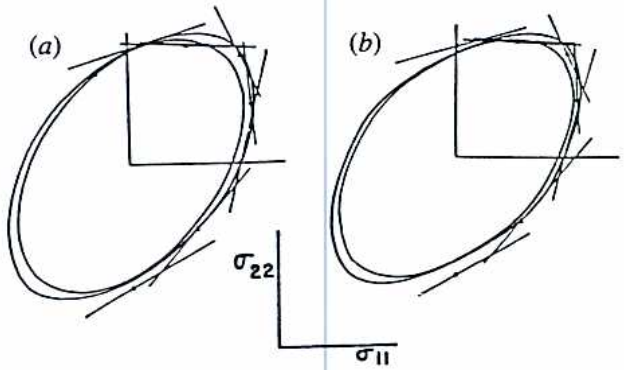

Fig. 10 — Comparison between the experimental (σ_{11}, σ_{22}) yield surface cross-sections of Althoff and Wincierz[21] and the predictions obtained from the (*a*) F_1 ($n = m = 1.7$) and (*b*) F_2 criteria for recrystallized Al tubes. Texture data from Ref. 21. The yield stresses have been normalized by the uniaxial yield stress σ_{11}.

the strain rates, as obtained from the normality rule. In this way, once the polycrystalline yield surface has been determined (see Section IV), yield stresses as well as Lankford coefficients can be assessed geometrically, as illustrated in Figure 11. The more direct methods described in Section II for the Taylor, Sachs, and Kochendörfer models, because of their computational simplicity, nevertheless lead to the more rapid assessment of the stress and strain rate properties.

A. *CMTP Predictions for Selected Ideal Orientations*

In this section, the strain rate and yield stress ratios pertaining to the main ideal orientations observed experimentally are first presented for the F_2 criterion. These single component simulations are then compared to experimental data reported in the literature. The two types of experiment represented by the 'not-strictly-uniaxial' ($\sigma_{12} \neq 0$) and uniaxial ($\dot{\varepsilon}_{12} \neq 0$) tensile tests (see Section II) are considered in turn. The former will be used in conjunction with the uniform strain model, and the latter with the Kochendörfer assumption. In Figure 12, $R(\theta)$ predictions are illustrated for the following ideal orientations: $\{100\}\langle 001\rangle$ (cube), $\{100\}\langle 011\rangle$, $\{100\}\langle 012\rangle$, $\{110\}\langle 001\rangle$ (Goss), $\{110\}\langle 112\rangle$ (Bs), $\{111\}\langle 1\bar{1}0\rangle$, $\{111\}\langle 11\bar{2}\rangle$, $\{112\}\langle 1\bar{1}0\rangle$, $\{112\}\langle 11\bar{1}\rangle$ (Cu), $\{123\}\langle 63\bar{4}\rangle$ (S), $\{146\}\langle 21\bar{1}\rangle$, and $\{554\}\langle 22\bar{5}\rangle$. By ideal orientation, we refer here to the group of four sets of Miller indices $\{hkl\}\langle uvw\rangle$, $\{h\,\bar{k}\,l\}\langle uvw\rangle$, $\{hkl\}\langle u\,\bar{v}\,w\rangle$, $\{h\,\bar{k}\,l\}\langle \bar{u}\,v\,w\rangle$ necessary to account for the symmetry of rolling.[11,22,23]

It is immediately apparent that some $R(\theta)$ characteristics widely observed experimentally are reproduced in these predictions; *i.e.*, a strong anisotropy is exhibited for the cube, Goss, Bs, Cu, S, and $\{554\}\langle 22\bar{5}\rangle$ orientations. Concurrently, nearly planar isotropy is predicted for the $\{111\}$ component. It is also of interest that the uniform strain assumption leads to $R(\theta)$ curves which are much less regular than those obtained from the Kochendörfer model (Figure 12). This is essentially due to the higher sensitivity to the detailed shape of the yield locus (which can be quite irregular in the case of the F_2 criterion; see Figure 3(b)) brought about by the use of the former type of interaction.

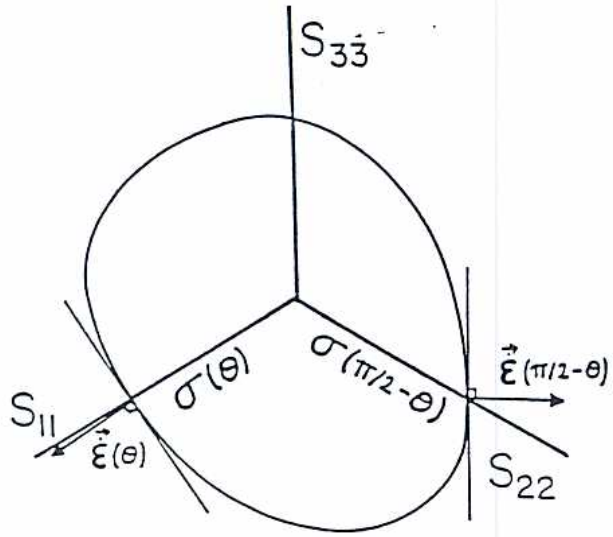

Fig. 11 — Calculation of the yield stress $\sigma(\theta)$ and strain rate $R(\theta)$ ratio from a yield surface. $\sigma(\theta)$ is the distance from the origin to the locus along the loading direction S_{11} and $R(\theta)$ is deduced from the normal to the surface at the loading point. $\sigma(\pi/2 - \theta)$ and $R(\pi/2 - \theta)$ are derived from the characteristics of the yield surface in the S_{22} direction.

It leads, for example, to the prediction of peaks in the case of the $\{111\}$ orientations which do not seem to be observed experimentally. For reference purposes, and for forecasting properties such as the limiting drawing ratio (LDR), the values of the average $\overline{R}$ as well as the planar ΔR strain rate ratios (as defined by Meuleman[24]) associated with each of the commonly observed ideal orientations are listed in Table I. It should be noted that certain texture components with a common $\{hkl\}$ plane have identical $\overline{R}$ and ΔR values (*e.g.*, $\{100\}\langle 001\rangle$ and $\{100\}\langle 011\rangle$) and others have different $\overline{R}$ and ΔR values (*e.g.*, $\{100\}\langle 001\rangle$ and $\{100\}\langle 012\rangle$). The reasons for these two kinds of behavior are discussed in Appendix I.

In Figure 13, some $R(\theta)$ predictions obtained with the F_2 function are compared with experimental data pertaining to highly textured sheet containing only one ideal orientation (plus the three symmetrical components). It can be seen that the Taylor and Kochendörfer analyses alternately give almost perfect agreement with these data and that they are both suitable for the estimation of the amplitudes as well as the average levels of the experimental $R(\theta)$ curves. Comparison of the present F_2 and two-exponent ($n = 2.6$, $m = 1.5$) F_1 results with the predictions published previously for the quadratic ($n = m = 2$[22]) and homogeneous non-quadratic ($n = m = 1.7$[11]) yield surfaces indicates that better and better predictions are obtained as the yield function is permitted to become more complex, *i.e.*, as it evolves from the quadratic, to the non-quadratic, to the two-exponent, to the homogeneous F_2 formulation, the latter containing terms with the products of stresses.

B. *Strain Rate and Yield Stress Ratio Predictions for Polycrystalline Materials*

The aim of this section is to illustrate the validity as well as the limitations of the CMTP method for predicting the $R(\theta)$ and $\sigma(\theta)/\sigma(0)$ curves pertaining to polycrystalline sheets. Only the Kochendörfer analysis (Section II–C) is used, as the uniform strain model involves more computation and leads to similar predictions. The former was applied to both the F_1 ($n = 2.6$, $m = 1.5$) and F_2 yield criteria (Eqs. [14] and [15]).

The texture data published by Hirsch *et al.*[18,25] (texture component + respective volume fraction) were used as inputs in the CMTP procedure. These data pertain to rolled (R), partially recrystallized (P), and fully recrystallized (F) Cu, Cu-5 pct Zn and Cu-20 pct Zn sheet. The $R(\theta)$ predictions are displayed in Figure 14, together with the experimental data of References 18 and 25, shown as bars. It can be seen that good quantitative agreement is obtained with the measured anisotropy in the case of the recrystallized materials. By contrast, the CMTP predictions underestimate some of the experimental values pertaining to the rolled sheet by a significant amount.

The copper-zinc system was also studied by Stephens,[26] whose experimental R-values are reported in Figure 15. The CMTP calculations based on the major texture components given in Reference 26 are seen to reproduce the measured anisotropy fairly closely. In contrast to the trends displayed in Figure 14 for similar materials, a slight *overestimation* of the Lankford coefficients is observed.

Two sets of data pertaining to bcc metals were also chosen so that the CMTP R-value predictions could be compared

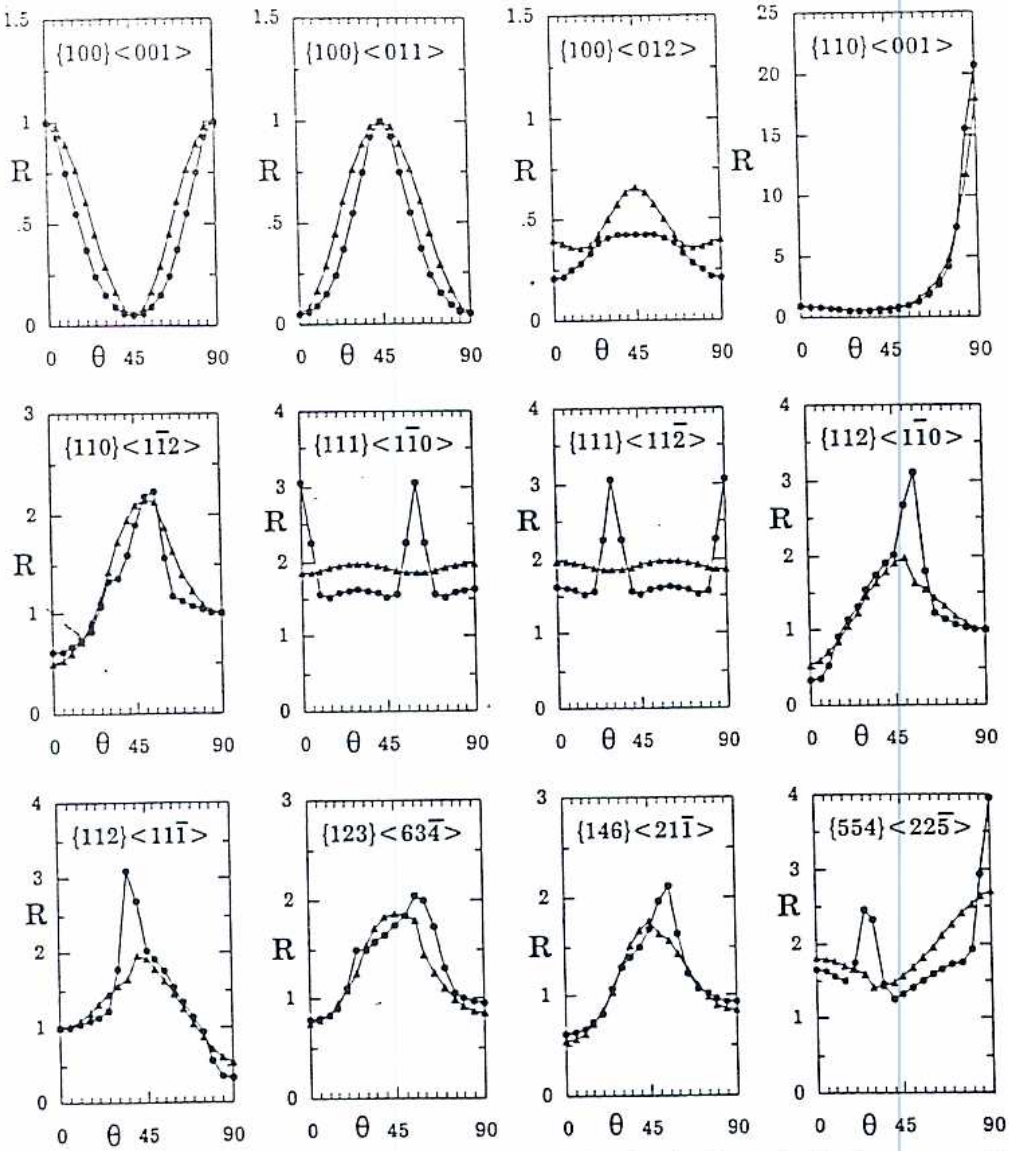

Fig. 12 — Values of $R(\theta)$ predicted by the CMTP method using the F_2 criterion for the common ideal orientations observed experimentally. The symmetry requirements of the rolling process have been taken into account: (—●—●—) Taylor assumption; (—▲—▲—) Kochendörfer model.

Table I. Average Strain Rate Ratios $\overline{R} = \{R(0) + 2R(5) + \ldots 2R(85) + R(90)\}/36$ and Planar Anisotropy Ratios $\Delta R = \{|R(0) - \overline{R}| + 2|R(5) - \overline{R}| + \ldots + 2|R(85) - \overline{R}| + |R(90) - \overline{R}|\}/36$ Predicted by the CMTP Method for the Main Ideal Orientations Observed Experimentally

Texture Component	$\overline{R}$		ΔR	
	Taylor Model	Kochendörfer Model	Taylor Model	Kochendörfer Model
{100}⟨001⟩	0.408	0.528	0.288	0.302
{100}⟨011⟩	0.408	0.528	0.288	0.302
{100}⟨012⟩	0.339	0.460	0.339	0.096
{110}⟨001⟩	2.873	2.688	3.041	2.702
{110}⟨1$\bar{1}$2⟩	1.240	1.351	0.386	0.464
{111}⟨1$\bar{1}$0⟩	1.814	1.913	0.357	0.035
{111}⟨11$\bar{2}$⟩	1.814	1.913	0.357	0.035
{112}⟨1$\bar{1}$0⟩	1.400	1.287	0.551	0.341
{112}⟨11$\bar{1}$⟩	1.400	1.287	0.551	0.341
{123}⟨63$\bar{4}$⟩	1.357	1.271	0.372	0.346
{146}⟨21$\bar{1}$⟩	1.195	1.138	0.358	0.332
{554}⟨22$\bar{5}$⟩	1.805	1.891	0.389	0.331

Account is taken of the symmetry requirements of rolling, and the F_2 yield criterion is used with both the Taylor and Kochendörfer grain interaction models.

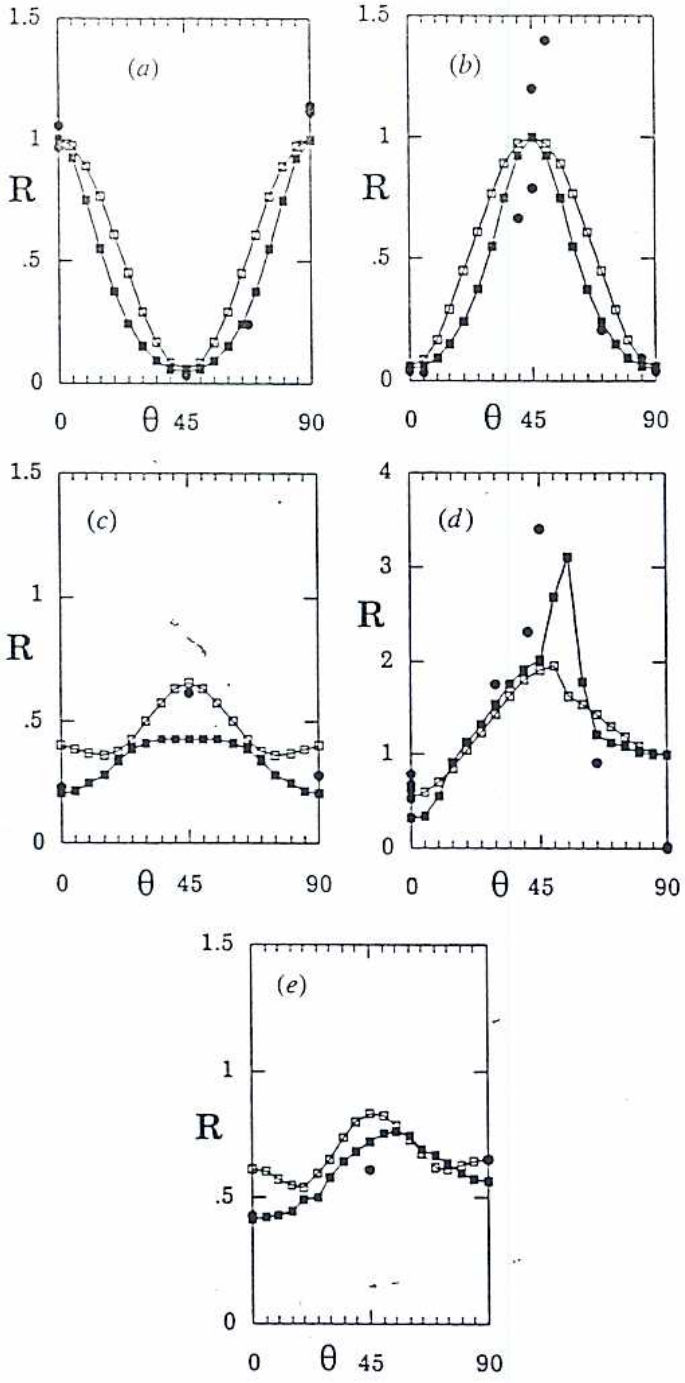

Fig. 13—Comparison of CMTP predictions (F_2 yield function) and experimental data (●) for various metals displaying the texture components indicated. (—■—) Taylor assumption; (—□—) Kochendörfer model. (*a*) Copper with a strong {100}⟨001⟩ texture.[13] (*b*) Iron single crystal sheet: {100}⟨011⟩ orientation.[19] (*c*) Cold rolled and annealed low C steel: {100}⟨012⟩ orientation.[35] (*d*) Iron single crystal sheet: {112}⟨1$\bar{1}$0⟩ orientation.[19] (*e*) Cold rolled and annealed low C steel: {411}⟨14$\bar{8}$⟩ orientation.[35]

with experimentally determined $R(\theta)$ curves. These are displayed in Figure 16, where the work of Ito *et al.*[27] is displayed, and in Figure 17, where the results of Parnière[19] are shown. It is evident from Figure 16(c) that the sharp R-value variation is accurately predicted. However, in the case of the other steels, the CMTP predictions underestimate the amplitudes of the $R(\theta)$ curves, although the positions of the R extrema are well reproduced. The relative inability of the present yield functions to reproduce the full extent of the R-variations can be readily explained by their smooth nature

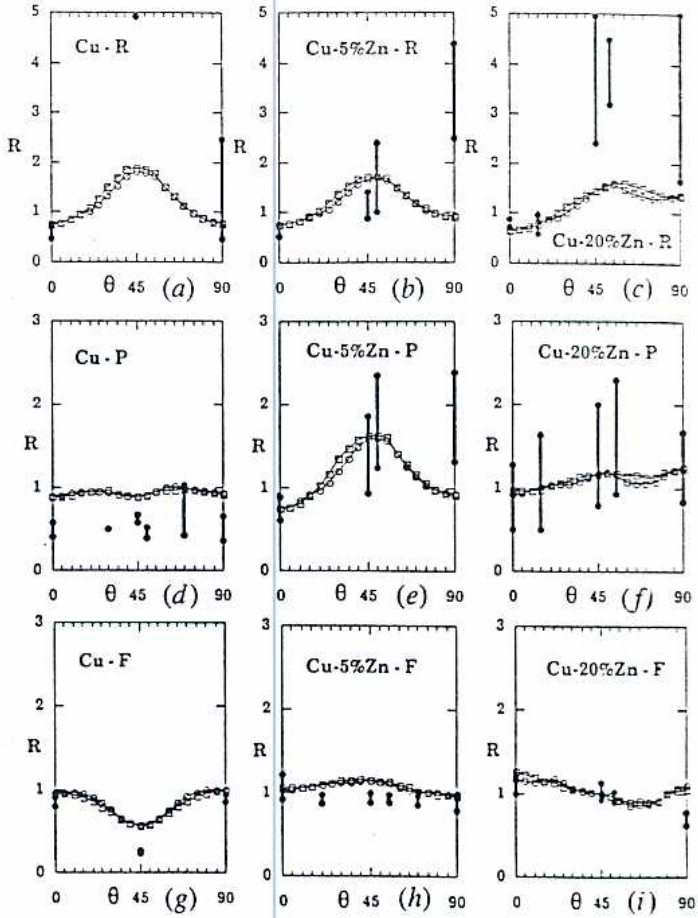

Fig. 14—$R(\theta)$ curves for the following rolled sheets: (*a*) Cu-R, (*b*) Cu-5 pct Zn-R, (*c*) Cu-20 pct Zn-R, (*d*) Cu-P, (*e*) Cu-5 pct Zn-P, (*f*) Cu-20 pct Zn-P, (*g*) Cu-F, (*h*) Cu-5 pct Zn-F, and (*i*) Cu-20 pct Zn-F. (●) Experimental R-values taken from Ref. 18. (—○○—) F_1 (n = 2.6, m = 1.5) and (—□□—) F_2 criteria used with the Kochendörfer model. The texture data used are those reported in Ref. 18.

(see Figures 7 through 10), which leads to reduced fluctuations in strain rate through the normality rule. By contrast, in crystallographic calculations,[12] the R-value variations are frequently too pronounced.

The results published by Stephens,[26] Kallend and Davies,[28,29] and Svensson[30,31] on yield stress measurements pertaining to cold rolled and annealed sheet are shown in Figures 18 through 20, respectively. The CMTP calculations carried out with both the F_1 (n = 2.6, m = 1.5) and F_2 criteria are also illustrated. In the first two cases, fairly good agreement is obtained between the experimental and theoretical stress ratios. Nevertheless, the anisotropy of yield strength determined by Svensson in aluminum sheets cold rolled to various reductions (Figures 20(a) and (b)) is considerably overestimated by the two criteria used. This can be attributed to the relative inability of the CMTP functions to reproduce the 'true' yield surface in shear stress space (see above).

VI. DISCUSSION

A. *Some Practical Uses of the CMTP Method*

The comparisons presented above between the CMTP and experimental $R(\theta)$ curves show that good agreement is ob-

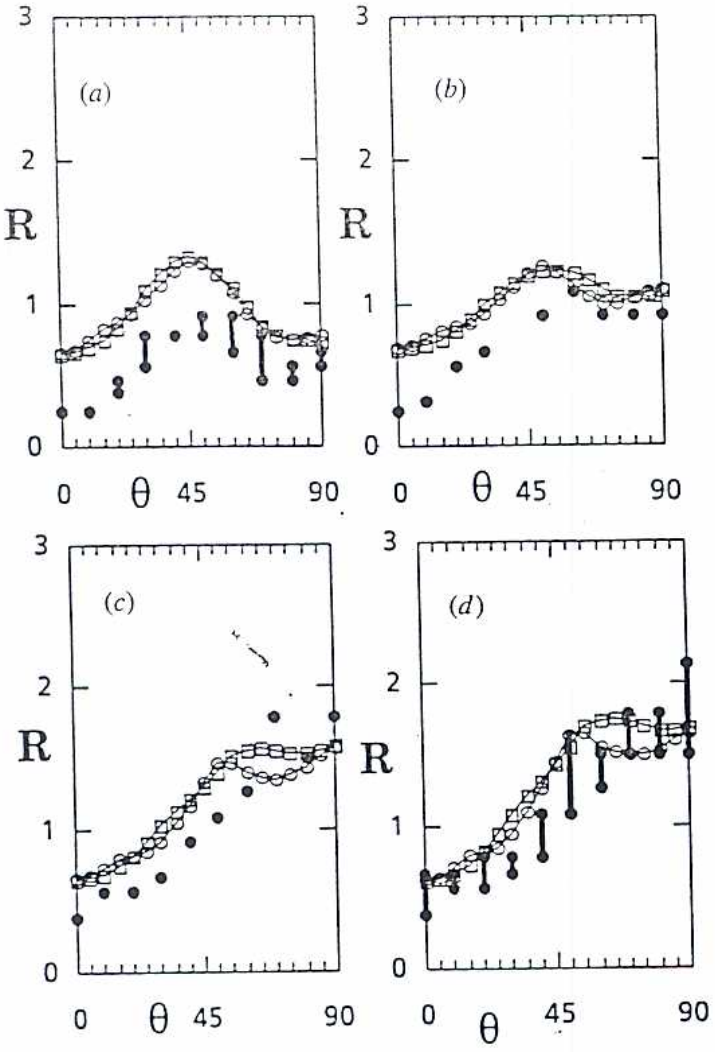

Fig. 15 — $R(\theta)$ curves for copper and brass sheets; (●) experimental R-values from Ref. 26. (—○○—) F_1 (n = 2.6, m = 1.5) and (—□□—) F_2 criteria used with the Kochendörfer model. The texture components employed are {311}⟨$\bar{1}$12⟩, {110}⟨1$\bar{1}$2⟩, and {110}⟨001⟩ in different volume fraction ratios.[26]

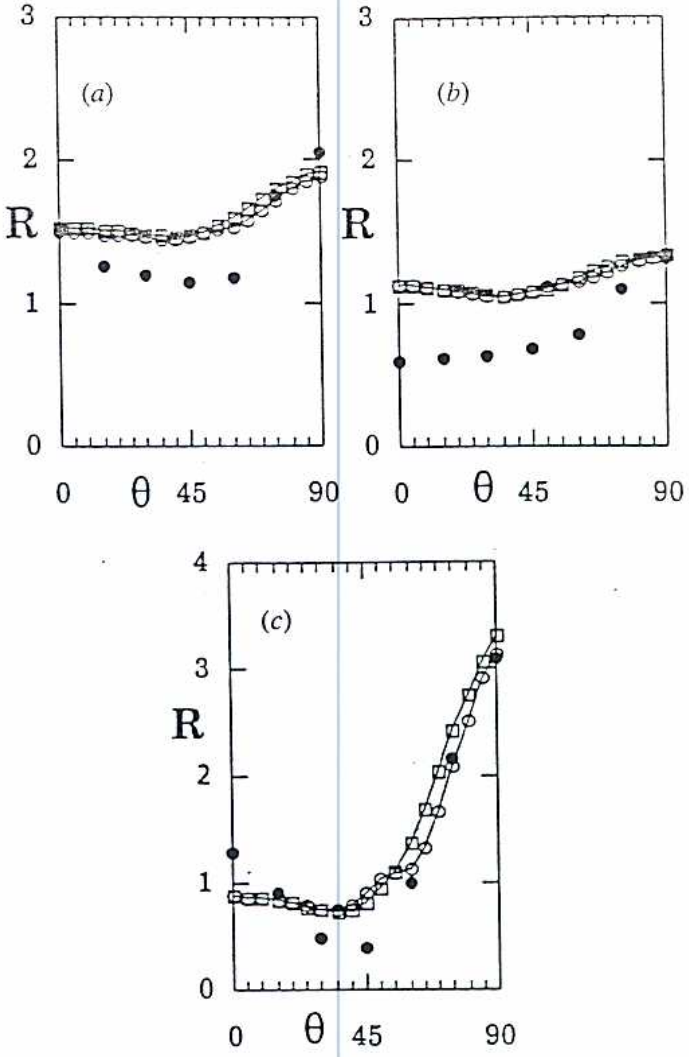

Fig. 16 — $R(\theta)$ curves for cold rolled steel sheet; (●) experimental R-values taken from Ref. 27. (—○○—) F_1 (n = 2.6, m = 1.5) and (—□□—) F_2 criteria used with the Kochendörfer model for steel sheets displaying (*a*) 60 pct {111}⟨0$\bar{1}$1⟩ + 10 pct {111}⟨11$\bar{2}$⟩ + 10 pct {110}⟨001⟩ + 20 pct random; (*b*) 10 pct {110}⟨001⟩ + 20 pct {111}⟨11$\bar{2}$⟩ + 70 pct random; and (*c*) 60 pct {110}⟨001⟩ + 20 pct {112}⟨1$\bar{1}$0⟩ + 20 pct random orientations.

served when only a few texture components (say 3 or 4 plus their rolling symmetries) need to be considered. The procedure can therefore be useful when the effects of the relative intensities of these 3 or 4 orientations must be assessed rapidly, such as for on-line applications. For such a purpose, 3 or 4 X-ray facilities oriented along 3 or 4 specific Bragg directions can be set up,[32] linked to a suitable microcomputer. The assessment of the relative weights of the texture components is in this case very fast, as is the CMTP estimation of the corresponding $R(\theta)$ and/or $\sigma(\theta)$ curves. The metallurgical parameters affecting the texture can consequently be adjusted on line until the desired anisotropy (or absence of anisotropy) is attained. For rolled fcc metals, the orientations that play a significant role are the Bs-{110}⟨1$\bar{1}$2⟩, S-{123}⟨63$\bar{4}$⟩, Cu-{112}⟨11$\bar{1}$⟩, and cube-{100}⟨001⟩ components; by contrast, the {100} and {111} types of textures have to be investigated in steel sheet.

Some data regarding the time required on an IBM PC AT microcomputer fitted with a DSI32 acceleration board to calculate the strain ratio $R(\theta)$, as well as the uniaxial $\sigma(\theta)$ and biaxial σ_b yield stresses pertaining to a single ideal orientation (including the four rolling symmetries) are listed in Table II. The homogeneous F_1 ($n = m = 1.7$),

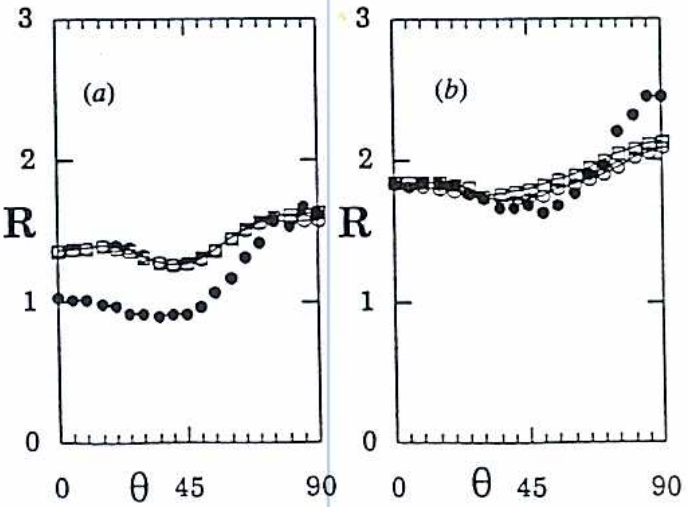

Fig. 17 — $R(\theta)$ curves for (*a*) an Al-killed steel and (*b*) a rimming steel; (●) experimental R-values taken from Ref. 19. (—○○—) F_1 (n = 2.6, m = 1.5) and (—□□—) F_2 criteria used with the Kochendörfer model for sheets displaying (*a*) 54 pct {111}⟨1$\bar{1}$0⟩ + 16 pct {111}⟨11$\bar{2}$⟩ + 30 pct {554}⟨22$\bar{5}$⟩; and (*b*) 46 pct {111}⟨1$\bar{1}$0⟩ + 23 pct {554}⟨225⟩ + 15 pct {310}⟨001⟩ + 8 pct {111}⟨11$\bar{2}$⟩ + 8 pct {100}⟨011⟩.

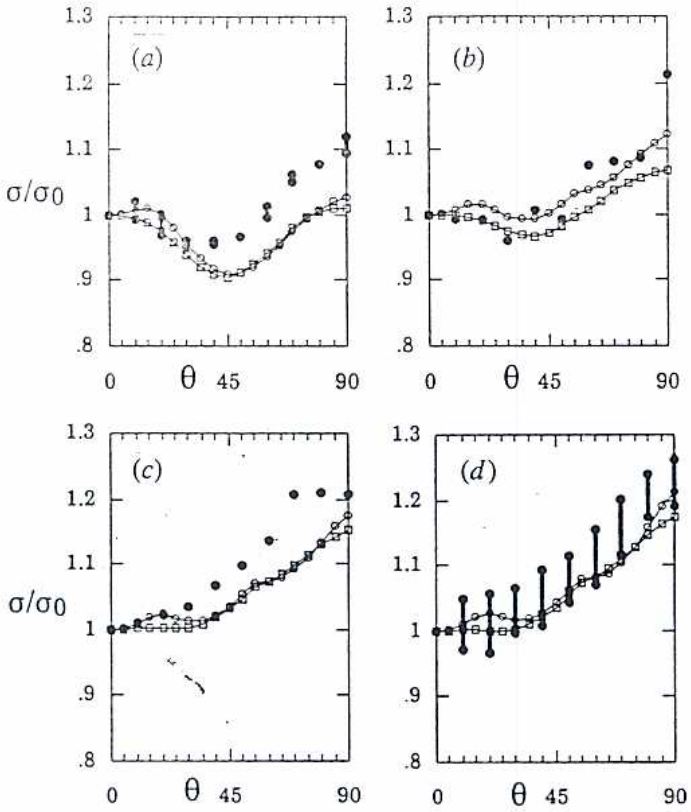

Fig. 18—Yield stress ratio $\sigma(\theta)/\sigma(0)$ curves for Cu and brass sheets; (•) experimental stress ratios taken from Ref. 26. (—○—○—) F_1 (n = 2.6, m = 1.5) and (—□—□—) F_2 criteria used with the Kochendörfer model. The texture components used are the {311}⟨1̄12⟩, {110}⟨1̄12⟩ and {110}⟨001⟩ orientations in different volume fraction ratios.

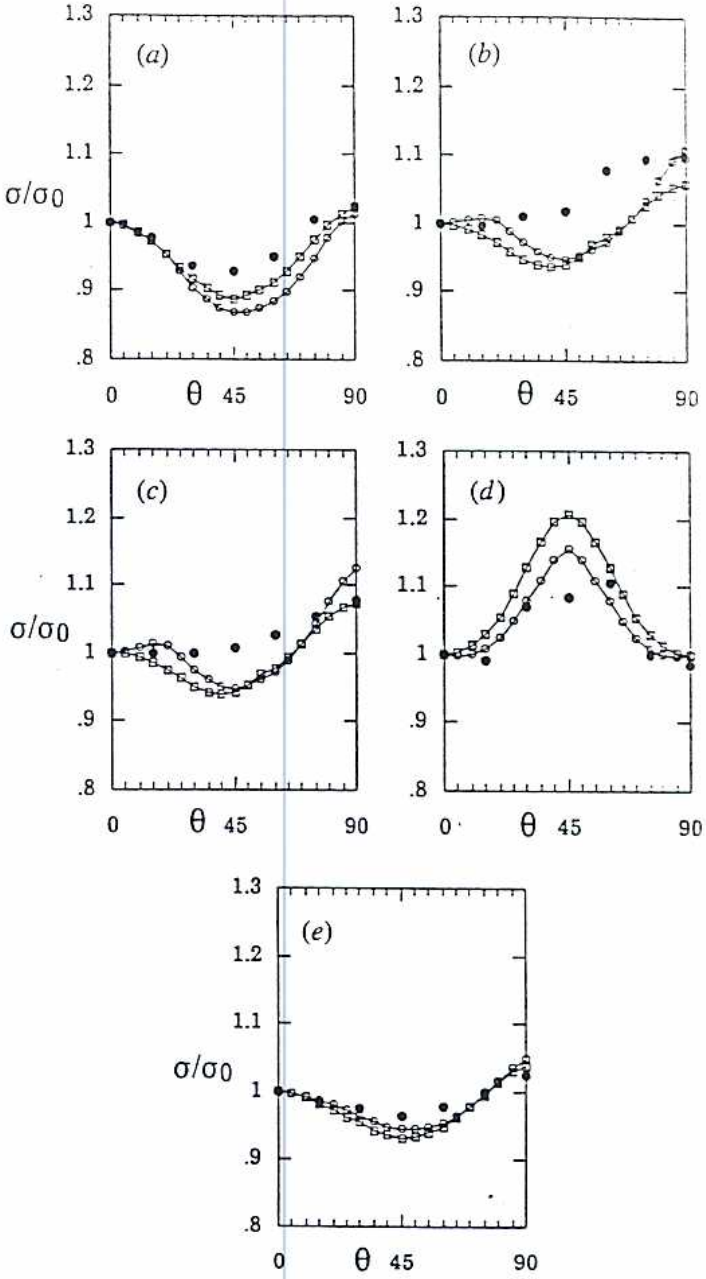

Fig. 19—Yield stress ratio $\sigma(\theta)/\sigma(0)$ curves for rolled and annealed Cu and brass; (•) experimental stress ratios taken from Refs. 28 and 29. (—○—○—) F_1 (n = 2.6, m = 1.5) and (—□—□—) F_2 criteria used with the Kochendörfer model for (*a*) Cu rolled to 90 pct reduction with 30 pct {110}⟨1̄12⟩ + 30 pct {123}⟨63̄4⟩ + 30 pct {112}⟨11̄1⟩ + 10 pct random; (*b*) Cu-10 pct Zn cold rolled to 90 pct reduction with 60 pct {110}⟨1̄12⟩ + 10 pct {123}⟨63̄4⟩ + 10 pct {111}⟨1̄10⟩ + 20 pct random; (*c*) Cu-30 pct Zn cold rolled to 90 pct reduction with 65 pct {110}⟨1̄12⟩ + 10 pct {123}⟨63̄4⟩ + 25 pct random; (*d*) annealed Cu with 70 pct {100}⟨001⟩ + 10 pct {100}⟨011⟩ + 20 pct random; and (*e*) annealed Cu-30 pct Zn with 20 pct {111}⟨11̄2⟩ + 20 pct {100}⟨011 − 20 pct {110}⟨1̄12⟩ + 40 pct random.

inhomogeneous $F_1(n = 2.6,\ m = 1.5)$, and F_2 yield criteria were used in conjunction with the (i) Taylor and (ii) Kochendörfer grain interaction models. The large differences observed are readily explained by the two-dimensional sweeping of strain rate space necessary in the case of the Taylor model, as well as by the numerical (as opposed to analytical) inversion of the normality rule required for the F_1 ($n = m = 1.7$) (as opposed to the F_2) criterion when employed in conjunction with the uniform strain hypothesis. By contrast, the Kochendörfer method leads to the rapid assessment of $R(\theta)$ and $\sigma(\theta)/\sigma(0)$ curves and appears to be particularly suitable for on-line measurements.

Another interesting application of the CMTP method involves the series development of the analytic expressions for the stress and strain rate components. For this purpose, the orientation distribution function $w(g)$ is used as a weighting factor in the calculation of the mean plastic properties pertaining to a polycrystalline aggregate. For example, the $R(\theta)$ value can be calculated according to the following averaging procedure:

$$R(\theta)_{(\text{polycrystal})} = \frac{\int w(g)\dot{\varepsilon}_{22}(\theta, g)\, dg}{\int w(g)\dot{\varepsilon}_{33}(\theta, g)\, dg} \qquad [21]$$

Here $\dot{\varepsilon}_{22}(\theta, g)$ and $\dot{\varepsilon}_{33}(\theta, g)$ are the CMTP expressions (which can be assessed using the Kochendörfer hypothesis) for the strain rate components corresponding to a given orientation g. A related technique has been employed at the Alcan Laboratories[33] in Kingston, Ontario, in which $R(\theta, g)$ (instead of $\dot{\varepsilon}_{22}(\theta, g)$ and $\dot{\varepsilon}_{33}(\theta, g)$ individually) is expanded directly and averaged using the OD function $w(g)$.

Finally, it should be noted that the CMTP method is well suited for FEM calculations. Most of the codes in service are based on isotropic, von Mises flow behavior. However, when an anisotropic starting material is used, or when a workpiece undergoes large prior deformation, anisotropic effects can strongly influence the flow when a further defor-

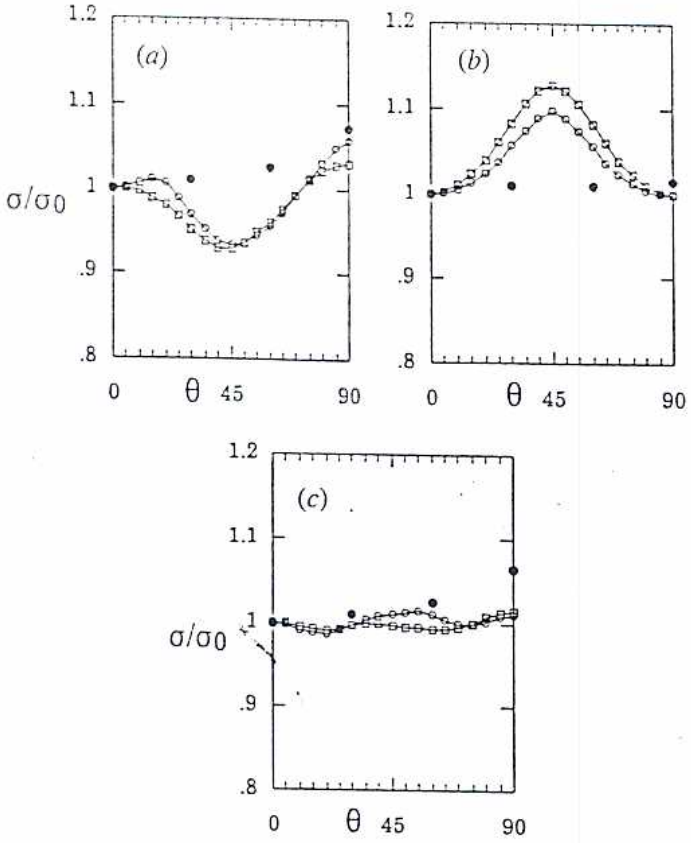

Fig. 20—Yield stress ratio $\sigma(\theta)/\sigma(0)$ curves for aluminum and steel sheets; (•) experimental stress ratios taken from Refs. 30 and 31. (—o—o—) F_1 ($n = 2.6$, $m = 1.5$) and (—□—□—) F_2 criteria used with the Kochendörfer model for (*a*) aluminum cold rolled to 80 pct reduction with 40 pct $\{311\}\langle\bar{1}12\rangle$ + 40 pct $\{110\}\langle1\bar{1}2\rangle$ + 20 pct random; (*b*) aluminum cold rolled to 10 pct reduction with 40 pct $\{100\}\langle001\rangle$ + 60 pct random; and (*c*) steel cold rolled to 80 pct reduction with 50 pct $\{113\}\langle1\bar{4}1\rangle$ + 30 pct $\{001\}\langle110\rangle$ + 20 pct random.

mation is applied. The employment of an anisotropic yield criterion of the CMTP type can considerably improve the accuracy of FEM calculations under these conditions without adding appreciable computing time.

B. *The CMTP Method: Advantages and Limitations*

(i) *Simplicity and rapidity of the procedure.* Once the main texture components of a deformed material are known, the CMTP technique provides a rapid way of assessing the corresponding $R(\theta)$ or $\sigma(\theta)$ curves. This is because the forms of the various functions allow the plastic strain rate properties to be expressed analytically in most cases. This is especially true when the Kochendörfer hypothesis is used (Section II–C), which leads to results comparable to those obtained from the considerably less direct Taylor grain interaction model.

Table II. Comparison of the Computing Times Necessary to Calculate $R(\theta)$ per Ideal Orientation (Symmetries Included) and per Angle θ, According to Different CMTP Criteria and Grain Interaction Models

Yield Criterion	Taylor Model	Kochendörfer Model
F_1 ($n = m = 1.7$)	6.32 sec	0.12 sec
F_1 ($n = 2.6$; $m = 1.5$)	—	0.17 sec
F_2	0.61 sec	0.06 sec

(ii) *Limited number of orientations required to represent textured materials.* The CMTP functions presented above describe the yield locus for a set of disoriented grains with an orientation spread of around 15 deg. For general polycrystal predictions, the texture of a given aggregate can be represented by the superposition of a limited number of such sets of grains, each with its own CMTP locus. By contrast, when the crystallographic method is employed, the full CODF must be used since the Bishop and Hill yield surface gives only the properties of a single cubic crystal. For the accurate prediction of $R(\theta)$, at least 600 grains are therefore necessary in the crystallographic approach,[4] whereas less than 10 (plus the rolling symmetries) are sufficient for the CMTP procedure.

(iii) *Acceptable $R(\theta)$ and $\sigma(\theta)$ predictions.* From all the comparisons carried out to date, it appears that the CMTP technique leads to good approximations of observed stress and strain rate ratios. The average $\bar{R}$-value (Table I) is generally better reproduced than the planar ΔR coefficient; *e.g.*, the high $R(\theta)$ variations observed in rolled fcc metals are frequently underestimated. This is essentially due to the smooth nature of the CMTP functions, which lead to smooth loci when the effects of several orientations present concurrently are combined.

(iv) *Yield surface predictions.* No final comment can be made here regarding the accuracy of the CMTP predictions of macroscopic yield loci. This is because a yield surface has five dimensions in stress space, whereas the experimentally determined yield strengths almost always pertain to two-dimensional sections and provide only a very limited representation of the overall yielding behavior. Nevertheless, the CMTP functions are unsuitable for reproducing the strain rate features of the very intensely textured materials which are almost equivalent to single crystals. In these cases, there is some experimental evidence for the presence of rounded corners on the yield surfaces,[13,21] a feature which is not reproduced by the present CMTP functions. When dealing with polycrystalline materials displaying larger dispersions around their various texture components, much better agreement is found (Figures 9 and 10).

(v) *Sources of error.* The analytic nature (and therefore the intrinsically ovoidal and ellipsoidal shapes of the yield surfaces) is the most attractive aspect of the present method as well as a source of error. However, the latter may not be large. Indeed, when the yield surfaces are compared with that pertaining to a set of disoriented grains,[4] a relatively good fit is observed, although the function is somewhat too smooth in certain regions, especially for highly textured aggregates. The determination of the main ideal orientations produced by rolling, and especially of their respective volume fractions, is also a source of error. Similarly, the percentage of the random component is difficult to estimate and generally plays a non-negligible role in the prediction of plastic anisotropy. Finally, errors are also associated with R-value measurement. These are in part due to the non-uniformity of the definitions found in the literature. The initial definition by Lankford *et al.*[34] referred to the ratio of the *total* strains in the width and thickness directions. However, the R-value expressed as a ratio of the *incremental* strains is more relevant to the present analysis, and to plas-

ticity theory in general. Experimentally, the R ratio depends on the amount of strain at which it is measured, which often varies from one investigation to another.[22]

VII. CONCLUSIONS

The CMTP (continuum mechanics of textured polycrystals) method, first introduced by Montheillet *et al.*[2] for the prediction of axial stresses in torsion testing, has been generalized to permit the calculation of plastic anisotropy in rolled sheet. New yield functions have been introduced, and three different averaging techniques have been employed to represent the various grain orientation distributions observed in rolled fcc and bcc metals. From this work, the following conclusions can be drawn:

1. Two types of continuum yield functions were derived according to the trends displayed by the crystallographic yield surfaces described in an earlier publication.[4] Of these, the two-exponent criterion F_1 ($n = 2.6, m = 1.5$) gives the best fit to the shear and normal stress behaviors. A second function F_2, based on a partial development of the equation of the Bishop and Hill polyhedron, gives a good fit to the π-plane and to a lesser degree to the shear stress plane cross-sections of the yield surface.
2. Yield surfaces as well as $R(\theta)$ and $\sigma(\theta)/\sigma(0)$ curves pertaining to polycrystalline materials were evaluated by considering three different grain interaction models: (i) the Taylor approach, in which all the grains are assumed to undergo the same strain as the polycrystal; (ii) the Sachs model, in which the stress direction is prescribed to be identical in all the grains of the aggregate; and (iii) the Kochendörfer hypothesis, in which the uniaxial stress direction as well as the value of the $\dot{\varepsilon}_{11}$ strain rate component are prescribed for all the crystals. Among these, the lattermost one, which allows for much faster computation than the Taylor approach because of an almost completely analytical description of yielding behavior, appears to be the most promising for industrial purposes.
3. Good agreement is observed between the predicted CMTP yield surface sections and experimental data for various metals when the orientations have dispersions of around 15 deg. However, the present method is unable to reproduce the rounded corners and flat edges of the experimental loci pertaining to polycrystals which are so sharply textured that they can be considered as near single crystals.
4. The strain rate $R(\theta)$ and yield stress $\sigma(\theta)/\sigma(0)$ ratios pertaining to rolled sheet were calculated for the common ideal orientations observed in both fcc and bcc metals. The general features of empirical $R(\theta)$ curves are given a ready analytical formulation in this way. When compared to experimental data pertaining to polycrystalline sheet, the CMTP calculations lead to good estimates of the $R(\theta)$ and $\sigma(\theta)/\sigma(0)$ curves. However, the average $\bar{R}$ value is generally better reproduced than its variation (ΔR) with angle θ, especially in the case of rolled fcc sheet. The positions of the extrema in the strain rate ratio curves (which give the locations of the ears in deep drawn cups) are also well approximated.
5. Finally, it is suggested that the F_2 and two-exponent F_1 ($n = 2.6$, $m = 1.5$) criteria can be readily used for on-line control purposes when a Kochendörfer (law of mixtures) analysis is employed. This is because the plastic anisotropy present in the material can be linked analytically and in a rapid way to the main texture components as well as to their respective weights.

APPENDIX I

Effect of $\{hkl\}$ of ideal orientation on $\bar{R}$ and ΔR

Two ideal orientations $\{hkl\}\langle uvw\rangle$ and $\{hkl\}\langle u'v'w'\rangle$ with a common $\{hkl\}$ direction parallel to the sheet normal are generally expected to have similar $\bar{R}$ and ΔR values. There are, however, numerous exceptions to this general rule, as will be seen below. For demonstration purposes, it is convenient to compare the $R(\theta)$ curves for the Goss ($\{110\}\langle 001\rangle$) and brass ($\{110\}\langle 1\bar{1}2\rangle$) texture components.

The $R(\theta)$ curve pertaining to the Goss $\{110\}\langle 001\rangle$ orientation, as given by the F_2 function, is illustrated in Figure A1(a). This orientation is one for which a single set of Miller indices is sufficient to respect the orthotropy conditions that apply to rolled sheet:[22]

$$R(-\theta) = R(\theta)$$
$$R(\pi-\theta) = R(\theta) \qquad [A1]$$

The $R(\theta)$ curve corresponding to the orientation $(110)[1\bar{1}2]$ is shown in Figure A1(b) (full line). This curve is similar to the previous one, but is displaced from it by an angle $\theta_0 \simeq 35$ deg (*i.e.*, the angle between the $\langle 001\rangle$ and $\langle 1\bar{1}2\rangle$ directions). It is evident, however, that the symmetry conditions of Eq. [A1] are not respected in this case. The latter requirements are generally satisfied by recognizing that an ideal orientation can consist of as many as four distinct orientations $(hkl)[uvw]$, $(\bar{h}\bar{k}l)[uvw]$, $(hkl)[\bar{u}\bar{v}w]$, and $(\bar{h}\bar{k}l)[\bar{u}\bar{v}w]$. Nevertheless, in the case of the brass orientation, only two sets of poles are necessary, *i.e.*, $(110)[1\bar{1}2]$ and $(\bar{1}\,\bar{1}0)[1\bar{1}2]$, whose $R(\theta)$ plots are displayed in Figure A1(b) (full and broken lines, respectively).

The R-value corresponding to the orthotropic texture $\pm(110)\pm[1\bar{1}2]$ can now be calculated by taking a suitable weighted (0.50) average over the two equivalent sets. For simplicity, we employ below the Kochendörfer analysis, although the Taylor approach could also have been used; this leads to:

$$R(\theta) = \frac{\dot{\varepsilon}_{yy}\{(110)[1\bar{1}2]\} + \dot{\varepsilon}_{yy}\{(\bar{1}\,\bar{1}0)[1\bar{1}2]\}}{\dot{\varepsilon}_{zz}\{(110)[1\bar{1}2]\} + \dot{\varepsilon}_{zz}\{(\bar{1}\,\bar{1}0)[1\bar{1}2]\}} \qquad [A2]$$

The $R(\theta)$ curve calculated in this way is depicted in Figure A1(c). It can be seen that the symmetry conditions of Eq. [A1] are obeyed, but that the shape and maximum amplitude of the composite $R(\theta)$ plot both differ considerably from the ones associated with the Goss component (Figure A1(a)). As a consequence, the $\bar{R}$ and ΔR values are also very different (see Table I). It can thus be concluded that the average $\bar{R}$ and planar ΔR strain rate ratios corresponding to two orthotropic textures having the same $\langle hkl\rangle$ direction parallel to the sheet are not necessarily similar.

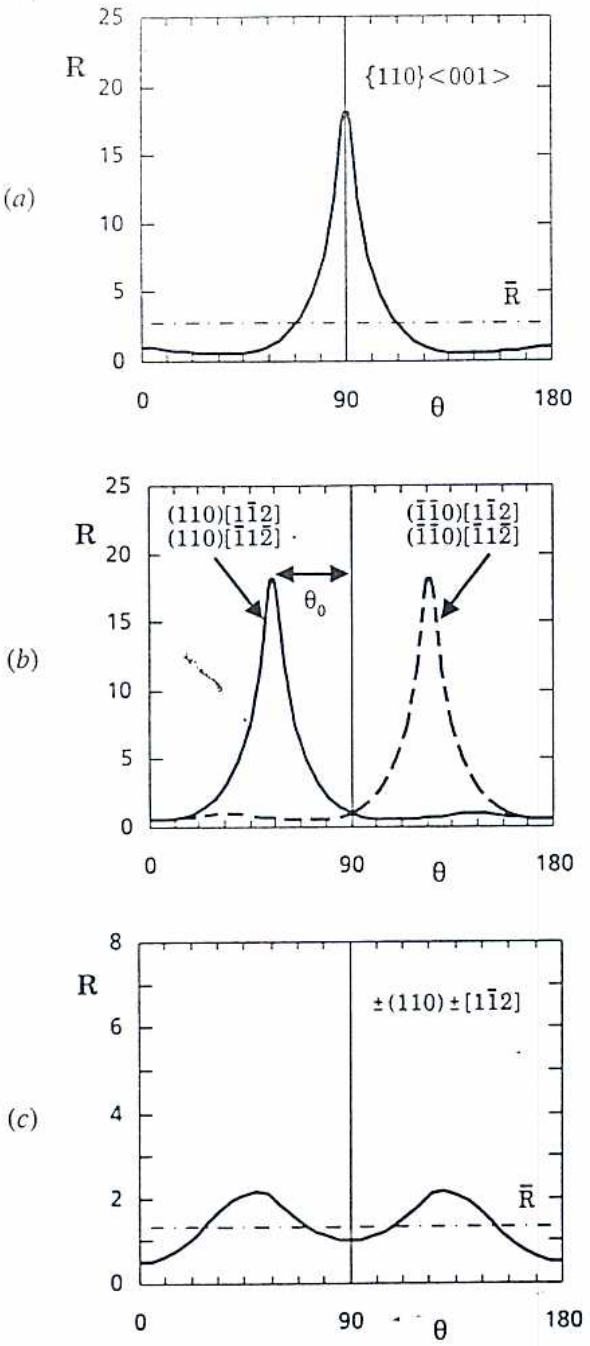

Fig. A1 — (*a*) $R(\theta)$ curve for the Goss texture ($\{110\}\langle 001\rangle$) as calculated using the Kochendörfer assumption and the F_2 yield function. Note that $\bar{R} \simeq 2.7$. (*b*) $R(\theta)$ curve calculated as in (a) for the (110) [1$\bar{1}$2] (full line) and ($\bar{1}\bar{1}$0) [1$\bar{1}$2] (broken line) components. These are shifted to the left and to the right, respectively, by about 35 deg with respect to the $R(\theta)$ curve in (a). (*c*) Average $R(\theta)$ curve for the $\{110\}\langle 1\bar{1}2\rangle$ texture as calculated from the yield surfaces pertaining to the two components required by the symmetry conditions. Note that $\bar{R} = 1.35$ differs from that obtained in (a) for the single component texture and that the scale has been changed.

The above reasoning can also be used to clarify the conditions under which different ideal orientations with a common $\{hkl\}$ plane are indeed associated with the same values of $\bar{R}$ and ΔR. This applies, for example, to single orientations that are both self symmetric and whose $R(\theta)$ curves therefore: (i) can be deduced without performing summations such as those of Eq. [A2]; and (ii) only differ by being displaced by the angle θ_0 corresponding to the rotation from $\langle uvw\rangle$ *to* $\langle u'v'w'\rangle$ (compare $\{100\}\langle 001\rangle$ and $\{100\}\langle 011\rangle$ in Table I). A variation of the above argument can be shown to apply to the other two component textures in Table I, namely the (111) [1$\bar{1}$0] and (111) [11$\bar{2}$] textures on the one hand, and the (112) [1$\bar{1}$0] and (112) [111] on the other. Here, each member of a particular pair is related to the other member by a simple rotation of $\theta_0 = 90$ deg and the type of summation involved in deducing the $R(\theta)$ curve is not changed by the rotation. Although not shown in detail here, these arguments can be extended to four component textures, including the ones shown in Table I.

In summary then, textures with common $\{hkl\}$ indices have the same $\bar{R}$ and ΔR values as long as (i) they belong to the same symmetry class (*i.e.*, when they all have either one, two, or four orientation components), and (ii) when, in the latter two cases, all the individual components are rotated by the same angle (*i.e.*, in a type of 'rigid body' rotation).

ACKNOWLEDGMENTS

The authors are indebted to Professor F. Montheillet as well as to Drs. B. Bacroix, J. H. Driver, R. Fortunier, and P. Gilormini for making a number of fruitful suggestions during the course of this work. They are particularly grateful to Professor W. F. Hosford for making the comment that led to the appendix, and to D. Daniel for his assistance in preparing it. They also acknowledge with gratitude the financial support received from the Natural Sciences and Engineering Research Council of Canada, The Quebec Ministry of Education (FCAR program), and the Canadian Steel Industry Research Association.

REFERENCES

1. P. Parnière and G. Pomey: 3rd Colloque Européen sur les Textures de Déformation et de Recristallisation de Métaux et leurs Applications Industrielles; Pont-à-Mousson, France, June 1973.
2. F. Montheillet, P. Gilormini, and J. J. Jonas: *Acta Metall.*, 1985, vol. 33, pp. 705-17.
3. G. R. Canova, U. F. Kocks, C. N. Tomé, and J. J. Jonas: *J. Mech. Phys. Solids*, 1985, vol. 33, pp. 371-97.
4. Ph. Lequeu, P. Gilormini, F. Montheillet, B. Bacroix, and J. J. Jonas: *Acta Metall.*, 1986, vol. 34, pp. 439-51.
5. G. I. Taylor: *J. Inst. Met.*, 1938, vol. 62, pp. 307-24.
6. P. van Houtte: *Texture and Microstructures*, 1987, vol. 7, pp. 29-72.
7. G. Sachs: *Z. d. Ver. deut. Ing.*, 1928, vol. 72, pp. 734-36.
8. Ph. Lequeu: Ph.D. Thesis, McGill University, Montreal, PQ, 1986.
9. A. Kochendörfer: *Reine und Angewandte Metallkde*, Springer, Berlin, 1941.
10. B. Bacroix and J. J. Jonas: *Textures and Microstructures*, in press.
11. Ph. Lequeu, P. Gilormini, F. Montheillet, B. Bacroix, and J. J. Jonas: *Acta Metall.*, 1987, vol. 35, pp. 1159-74.
12. Ph. Lequeu, F. Montheillet, and J. J. Jonas: in *Symp. on Computer Modelling of Fabrication Processes and Constitutive Behaviour of Metals*, Ottawa, ON, Canada, J. J. M. Too *et al.*, eds., 1986, pp. 237-66.
13. C. S. da C. Viana, J. S. Kallend, and G. J. Davies: *Int. J. Mech. Sci.*, 1979, vol. 21, pp. 355-71.
14. R. Sowerby, C. S. da C. Viana, and G. J. Davies: *Mats. Sci. Engng.*, 1980, vol. 46, pp. 23-51.
15. W. F. Hosford: *J. Appl. Mech. (Trans. ASME ser. E)*, 1972, vol. 39, pp. 607-09.
16. R. W. Logan and W. F. Hosford: *Int. J. Mech. Sci.*, 1980, vol. 22, p. 419.
17. W. F. Hosford: *Proc. 7th North American Metalworking Conf., SME*, Dearborn, MI, 1979, p. 191.

18. J. Hirsch, R. Musick, and K. Lücke: in *Fifth Int. Conf. on Textures of Materials*, Aachen, Germany, G. Gottstein and K. Lücke, eds., Springer, Berlin, 1978, vol. II, pp. 437-46.
19. P. Parnière: Thèse, Docteur Es-Sciences Phys., Centre d'Orsay, Université de Paris Sud, 1978.
20. J. L. Bassani: *Int. J. Mech. Sci.*, 1977, vol. 19, pp. 651-60.
21. J. Althoff and P. Wincierz: *Z. Metallkde*, 1972, vol. 63, pp. 623-33.
22. Ph. Lequeu, F. Montheillet, and J. J. Jonas: in *Symp. on Textures in Nonferrous Metals and Alloys*, Detroit, MI, H. D. Merchant and J. G. Morris, eds., TMS-AIME, 1984, pp. 189-212.
23. M. Hatherley and W. B. Hutchinson: in *An Introduction to Textures in Metals*, Chameleon Press Ltd., The Institution of Metallurgists, 1979.
24. D. J. Meuleman: Ph.D. Thesis, University of Michigan, Ann Arbor, MI, 1980.
25. J. Hirsch: Diplomarbeit, Rheinische, Westfälische Technische Hochschule Aachen, Germany, 1978.
26. A. W. Stephens: Ph.D. Thesis, University of Arizona, Tucson, AZ, 1968.
27. Y. Ito, K. Hashiguchi, and N. Ohashi: in *Int. Conf. on the Science and Tech. of Iron and Steel*, Trans. Iron and Steel Inst. Japan, 1971, p. 958.
28. J. S. Kallend and G. J. Davies: *J. Inst. Metals*, 1970, vol. 98, pp. 242-44.
29. J. S. Kallend and G. J. Davies: *J. Inst. Metals*, 1971, vol. 5, pp. 257-60.
30. N. L. Svensson: *J. Inst. Met.*, 1966, vol. 94, pp. 284-91.
31. N. L. Svensson: *Trans. AIME*, 1966, vol. 236, pp. 1004-09.
32. J. Hirsch: Institut für Allgemeine Metallkunde und Metallphysik, RWTH Aachen, West Germany, private communication, 1986.
33. M. Bull and D. J. Lloyd: ALCAN Lab., Kingston, ON, unpublished work, 1986.
34. W. T. Lankford, S. C. Snyder, and J. A. Bauscher: *Trans. Am. Soc. Metals*, 1950, vol. 42, pp. 1197-1232.
35. J. A. Elias, R. H. Heyer, and J. G. Smith: *Trans. AIME*, 1962, vol. 224, pp. 678-86.